Raman Spectroscopy of DNA-Metal Complexes. II. The Thermal Denaturation of DNA in the Presence of Sr^{2+}, Ba^{2+}, Mg^{2+}, Ca^{2+}, Mn^{2+}, Co^{2+}, Ni^{2+}, and Cd^{2+}

John G. Duguid,* Victor A. Bloomfield,* James M. Benevides,‡ and George J. Thomas, Jr.‡
*Department of Biochemistry, University of Minnesota, St. Paul, Minnesota 55108, and ‡Division of Cell Biology and Biophysics, School of Biological Sciences, University of Missouri-Kansas City, Kansas City, Missouri 64110 USA

ABSTRACT Differential scanning calorimetry, laser Raman spectroscopy, optical densitometry, and pH potentiometry have been used to investigate DNA melting profiles in the presence of the chloride salts of Ba^{2+}, Sr^{2+}, Mg^{2+}, Ca^{2+}, Mn^{2+}, Co^{2+}, Ni^{2+}, and Cd^{2+}. Metal-DNA interactions have been observed for the molar ratio $[M^{2+}]/[PO_2^-] = 0.6$ in aqueous solutions containing 5% by weight of 160 bp mononucleosomal calf thymus DNA. All of the alkaline earth metals, plus Mn^{2+}, elevate the melting temperature of DNA ($T_m > 75.5°C$), whereas the transition metals Co^{2+}, Ni^{2+}, and Cd^{2+} lower T_m. Calorimetric (ΔH_{cal}) and van't Hoff (ΔH_{VH}) enthalpies of melting range from 6.2–8.7 kcal/mol bp and 75.6–188.6 kcal/mol cooperative unit, respectively, and entropies from 17.5 to 24.7 cal/K mol bp. The average number of base pairs in a cooperative melting unit ($\langle n_{melt} \rangle$) varied from 11.3 to 28.1. No dichotomy was observed between alkaline earth and transition DNA-metal complexes for any of the thermodynamic parameters other than their effects on T_m. These results complement Raman difference spectra, which reveal decreases in backbone order, base unstacking, distortion of glycosyl torsion angles, and rupture of hydrogen bonds, which occur after thermal denaturation. Raman difference spectroscopy shows that transition metals interact with the N7 atom of guanine in duplex DNA. A broader range of interaction sites with single-stranded DNA includes ionic phosphates, the N1 and N7 atoms of purines, and the N3 atom of pyrimidines. For alkaline earth metals, very little interaction was observed with duplex DNA, whereas spectra of single-stranded complexes are very similar to those of melted DNA without metal. However, difference spectra reveal some metal-specific perturbations at 1092 cm^{-1} (nPO_2^-), 1258 cm^{-1} (dC, dA), and 1668 cm^{-1} (nC═O, dNH_2 dT, dG, dC). Increased spectral intensity could also be observed near 1335 cm^{-1} (dA, dG) for CaDNA. Optical densitometry, employed to detect DNA aggregation, reveals increased turbidity during the melting transition for all divalent DNA-metal complexes, except SrDNA and BaDNA. Turbidity was not observed for DNA in the absence of metal. A correlation was made between DNA melting, aggregation, and the ratio of Raman intensities I_{1335}/I_{1374}. At room temperature, DNA-metal interactions result in a pH drop of 1.2–2.2 units for alkaline earths and more than 2.5 units for transition metals. Sr^{2+}, Ba^{2+}, and Mg^{2+} cause protonated sites on the DNA to become thermally labile. These results lead to a model that describes DNA aggregation and denaturation during heating in the presence of divalent metal cations: 1) The cations initially interact with the DNA at phosphate and/or base sites, resulting in proton displacement. 2) A combination of metal-base interactions and heating disrupts the base pairing within the DNA duplex. This allows divalent metals and protons to bind to additional sites on the DNA bases during the aggregation/melting process. 3) Strands whose bases have swung open upon disruption are linked to neighboring strands by metal ion bridges. 4) Near the midpoint of the melting transition, thermal energy breaks up the aggregate. We have no evidence to indicate whether metal ion cross-bridges or direct base-base interactions rupture first. 5) Finally, all cross-links break, resulting in single-stranded DNA complexed with metal ions.

INTRODUCTION

Our objective in this paper is to characterize and compare the structural and thermodynamic changes that DNA undergoes upon thermal melting in the presence of the divalent alkaline earths Sr^{2+}, Ba^{2+}, Mg^{2+}, and Ca^{2+} and transition metals Mn^{2+}, Co^{2+}, Ni^{2+}, and Cd^{2+}. We present a variety of evidence leading to a five-step mechanism, with specific involvement of divalent cations at each step, proceeding from double-stranded B-DNA at room temperature to single-stranded DNA above the melting temperature.

Early UV-visible spectrophotometry (Anderson et al., 1971; Dix and Straus, 1972; Dove and Davidson, 1962; Eichhorn and Clark, 1965; Eichhorn and Shin, 1968; Shin and Eichhorn, 1968; Zimmer et al., 1974) and circular dichroism (Luck and Zimmer, 1972; Zimmer et al., 1974) studies showed that duplex DNA is stabilized by alkaline earth metals against thermal or acid denaturation and destabilized by transition metals. From these experiments, it was concluded that alkaline earths interact primarily with the DNA phosphates, stabilizing the double helix through reduced charge repulsion of its complementary strands. This is supported by Raman studies which showed that Ca^{2+} and Mg^{2+} interact primarily with the ionic phosphates and show little interaction with the bases (Langlais et al., 1990). Similarly, proton nuclear magnetic resonance (NMR) and Fourier transform infrared spectroscopy studies of interac-

Received for publication 12 October 1994 and in final form 31 August 1995.

Address reprint requests to Dr. Victor A. Bloomfield, Department of Biochemistry, University of Minnesota, 1479 Gortner Avenue, St. Paul, MN 55108. Tel.: 612-625-2268; Fax: 612-625-6775; E-mail: victor@molbio.cbs.umn.edu.

This is Part LV in the series Raman Spectral Studies of Nucleic Acids.

0006-3495/95/12/2623/19 $2.00

tions between guanylic acid and the alkaline earths in solution indicated that the metals do not interact directly with the bases (Tajmir-Riahi, 1991). Equilibrium binding experiments using colorimetric assays established that Ca binding to DNA is independent of base sequence and can be described by polyelectrolyte theory (Manzini et al., 1990).

There is some evidence, however, that alkaline earth metal ions do bind to DNA bases, or at least influence them indirectly. For example, they enhance base stacking, probably by reducing electrostatic repulsion along the DNA chain (Langlais et al., 1990). Crystallographic studies show coordination between hydrated shells of Mg^{2+} and guanine bases of Z-DNA (Gessner et al., 1985). ^{43}Ca-NMR studies show that at low calcium-to-DNA phosphate ratios, Ca^{2+} binds tightly to DNA in a way not well described by electrostatics (Braunlin et al., 1987, 1989). In the present work, we observe an extent of deprotonation of DNA, when alkaline earths are added, that cannot be accounted for by terminal phosphates or by hydrolysis of the cations. Alkaline earths also influence sugar conformations. The ribose moieties of Mg, Ca, and Sr-GMP complexes have a C3′-*endo/anti* sugar pucker, whereas the Ba-GMP complex is C2′-*endo/anti* (Tajmir-Riahi, 1991). Thus, even though the alkaline earths interact predominantly with the DNA phosphates, they also have effects on other parts of the DNA structure.

Transition metals destabilize duplex DNA through their greater affinity for the nitrogenous bases, with the most reactive site being the N7 atom of guanine (Daune, 1974). Binding of Cd^{2+} at guanine N7 has been verified by crystallographic studies on GMP (Aoki, 1976) and by infrared spectroscopy of both B and Z forms of poly(dG-dC) (Keller et al., 1988). The latter study also suggests binding of Cd^{2+} to the N3 of guanine. However, binding at N3 is not likely because of steric constraints imposed by the sugar residue (Eichhorn, 1981). NMR studies (Anderson et al., 1971; Van Steenwinkel et al., 1981), which investigated the relaxation rates of water protons in the presence of MnDNA, showed that Mn has an affinity for GC residues with a preference for the N7 atom of guanine. A Raman study of divalent metal interactions with GMP suggests that nickel binds to the N7 atom of guanine and is stabilized by chelation of the phosphate group (Makrigiannis et al., 1980). Langlais et al. (1990) have interpreted Raman spectra of calf thymus DNA in the presence of Cd^{2+} to indicate binding to phosphates and AT regions, as well as to the N7 atom of guanine. At [Cd^{2+}]:[phosphate] ratios of 5:1, Cd^{2+} induces base unstacking, backbone disordering, and perturbations of carbonyl modes that are normally associated with DNA melting. Duguid et al. (1993) have shown that Mn^{2+}, Ni^{2+}, and Cd^{2+} interact extensively with acceptor sites on the purine (N7) and pyrimidine (N3) rings and destabilize concentrated solutions of high-molecular-weight DNA at room temperature.

Sedimentation experiments (Zimmer et al., 1974) and solubility assays utilizing UV-visible spectrophotometry (Knoll et al., 1988) show that divalent metals also cause DNA aggregation at elevated temperatures. Two models were proposed for DNA aggregation (Knoll et al., 1988). The first involves aggregation of intact, duplex DNA, whereas the second postulates partial separation of the DNA strands. Mechanisms requiring complete melting before aggregation were ruled out on the basis of S1 nuclease assays of the redissolved aggregates. A relationship between melting and aggregation of MgDNA was implied by studies (Ott, 1975; Ott et al., 1978) that showed multiphasic optical melting transitions, some of which involved aggregate formation confirmed by electron microscopy.

In this paper we use differential scanning calorimetry (DSC) to evaluate thermodynamic parameters associated with the melting of 160-bp fragments of calf thymus DNA in the presence of the chloride salts of Sr, Ba, Mg, Ca, Mn, Co, Ni, and Cd. We employ Raman spectroscopy and optical densitometry to identify secondary structural perturbations and aggregate formation over the temperature range 20–93°C. Over this same range, we combine pH potentiometry with Raman difference spectroscopy to identify DNA binding sites and structural changes associated with DNA-metal complexation. The integrated results from these four experimental approaches provide a comprehensive perspective on the interactions of divalent cations with DNA, the nature of changes in secondary, tertiary and quaternary structures induced by these metals, and the thermodynamic parameters governing the behavior of their complexes with DNA.

MATERIALS AND METHODS

Salt solutions

Chloride salts of the divalent cations were obtained from Aldrich Chemical (Milwaukee) and used without further purification. Stock solutions containing 200 mM of the metal salt and 5 mM sodium cacodylate were adjusted to pH 6.5 with HCl.

Preparation of DNA

Mononucleosomal calf thymus DNA (160 ± 5 bp) was prepared using methods previously described (Strzelecka and Rill, 1987; Wang et al., 1990) and purified by three successive phenol extractions. One and a half volumes of cold isopropanol (−20°C) was added to the aqueous DNA-containing layer, and the mixture was stored overnight at −20°C. The precipitated DNA was removed by centrifugation at 8000 rpm in a Beckman JA-10 rotor for 45 min, dried, and resuspended in 10 mM Na_2HPO_4 + 0.2 M NaCl + 1 mM Na_2EDTA (pH 7.5). The solution was dialyzed twice against 4 M NaCl + 5 mM EDTA (pH = 7.5), twice against 1 M NaCl (pH = 7.5), and four times against Milli-Q water, and then lyophilized. The lyophilizate was desiccated at −20°C. To prepare each DNA-metal complex, DNA was dissolved to 5% w/w in a solution containing 100 mM metal chloride + 5 mM sodium cacodylate (pH 6.5), yielding a divalent metal cation-to-phosphate molar ratio [M^{2+}]/[PO_2^-] of 0.6. Solutions were maintained at 4°C overnight. These solution conditions were used for all experiments described below.

Differential scanning calorimetry

Solutions of DNA complexes were saturated with helium for 30 min to reduce bubble formation upon heating. One and a half milliliters of the DNA sample and reference buffer were loaded into their appropriate

reservoirs in a MicroCal MC-2 differential scanning calorimeter (Amherst, MA) using a 3 cm^3 Hamilton syringe (Reno, NV). An external pressure of 40 psi was applied to the sample, and reference cells were cooled to 10°C with a computer-controlled Haake F3-CH circulator (Paramus, NJ). The sample was scanned relative to the reference buffer over the temperature range from 10°C to 98°C at a scan rate of 12 K h^{-1}. Data were obtained using the DA-2 acquisition system (MicroCal) under the control of an IBM personal computer that was interfaced to the calorimeter through a Data Translation AT 2801 IO board (Marlboro, NH). Heat capacity plots were cell- and baseline-corrected according to standard techniques that have been discussed extensively (Hinz, 1986; Privalov and Potakhin, 1986; Sturtevant, 1987). The integrated enthalpy $\Delta H(T)$, used to estimate the extent of DNA melting, was obtained by integrating the measured heat capacity relative to the reference solution in the absence of the DNA (ΔC_p) with respect to temperature. ΔH_{cal} and ΔS_{cal} were obtained from the total areas under the ΔC_p versus T and $\Delta C_p/T$ versus T curves, respectively. T_m was then determined from the equilibrium condition

$$T_m = \Delta H_{cal}/\Delta S_{cal}. \quad (1)$$

The van't Hoff enthalpy (ΔH_{VH}) was obtained from the relation

$$\Delta H_{VH} = 6RT_m^2 \frac{\Delta C_p(T_m)}{\Delta H_{cal}}, \quad (2)$$

where R is the gas constant and $\Delta C_p(T_m)$ is the measured value of the heat capacity at T_m relative to the reference solution in the absence of the DNA. Note that for helix-coil transitions of DNA, $C_p(\text{coil}) - C_p(\text{helix}) = 0$ (Marky and Breslauer, 1987). The average number of base pairs, $\langle n_{melt} \rangle$, in a cooperative melting unit was calculated from the ratio

$$\langle n_{melt} \rangle = \Delta H_{VH}/\Delta H_{cal}. \quad (3)$$

We evaluated the apparent cooperativity parameter (σ) using helix-coil transition theory (Cantor and Schimmel, 1980). The equilibrium constant for helix propagation (s) is determined as a function of T from

$$\ln(s) = \frac{\Delta H_{cal}}{R}\left(\frac{1}{T} - \frac{1}{T_m}\right). \quad (4)$$

According to helix-coil transition theory, the fractional extent of melting is

$$\theta = \left(\frac{s}{2\lambda}\right)\left(1 + \frac{s - 1 + 2\sigma}{[(1-s)^2 + 4\sigma s]^{1/2}}\right), \quad (5)$$

where

$$\lambda = \tfrac{1}{2}\{(1+s) + [(1-s)^2 + 4\sigma s]^{1/2}\}. \quad (6)$$

After substituting values of θ_{exp} and s into Eqs. 5 and 6, we adjusted σ until the best fit was obtained. Back-substitution of σ allowed calculation of θ for comparison with experimental measurements. The helix-coil transition theory applies rigorously only to polymers of infinite length, and we acknowledge that its application to 160-bp fragments of calf thymus DNA is an approximation of the data. In addition, our determination of σ does not include sequence specificity and serves only as an apparent determination of σ. Nonetheless, the value of σ obtained provides an empircal measure of the cooperativity of the metal-DNA complex that is inevitably related to the free energy of base stacking.

Raman difference spectroscopy

The DNA-metal complexes were mixed to homogeneity, and 10-μl aliquots were sealed in glass capillary tubes (Kimax, art. no. 34502) for Raman analysis. The Raman spectra were excited with the 514.5 nm line of an argon laser (Coherent Innova 70) using approximately 200 mW of radiant power at the sample. The spectra were collected on a triple spectrograph (Spex Instruments, model 1877 Triplemate) equipped with an intensified diode array detector (EG and G Princeton Applied Research, OMA-III). Data were collected on thermostated samples at approximately 5°C increments between 20°C and 93°C. To improve Raman signal-to-noise ratios, up to several hundred accumulated exposures were averaged over the spectral interval 600-1750 cm^{-1}. Weak background scattering by the aqueous solvent was removed using computer subtraction techniques in which intensities at 786, 1014, and 1622 cm^{-1} were normalized relative to a water-corrected spectrum of B-DNA in H_2O at the same temperature. This approach retains the fidelity of the relative Raman intensities of B-DNA established previously (Prescott et al., 1984), which were confirmed by applying standard solvent corrections to spectra recorded independently on a scanning spectrometer (Spex Ramalog).

Optical densitometry

DNA-metal complexes were mixed to homogeneity, sealed in glass capillary tubes, and thermostated at the appropriate temperature. Optical densities were measured in the transmittance mode with a GS300 scanning densitometer (Hoefer Scientific Instruments, San Francisco). A digital multimeter (Simpson, model 464), connected to the scanning densitometer, allowed the measurement of resistance as a function of sample turbidity. Resistance was measured at 2–5°C intervals over the temperature range 20–95°C on the same DNA-metal sample preparations investigated by DSC and Raman difference spectroscopy. A turbidity curve was obtained by plotting the temperature dependence of the measured resistance values. To further analyze the extent of aggregation, we integrated the turbidity curve with respect to temperature. The resulting integrated turbidity curve was compared to the $\Delta H(T)$ curve (obtained from DSC) to evaluate the extent of overlap between melting and aggregation of the DNA-metal complexes.

pH potentiometry

DNA-metal complexes were mixed to homogeneity in 1.5-ml Eppendorf tubes and thermostated at the appropriate temperature. pH was measured with a Wilmad combination pH electrode (model 6030-02) and a Markson solution analyzer (model 4603) over the temperature range 25–95°C. A pH titration curve was acquired for each DNA-metal complex to compare with its turbidity and ΔH curves. The number of solution protons absorbed onto the DNA during a thermal transition or released during metal complexation was determined from the equation

$$\Delta[H^+]_{soln} = 10^{-pH_1} - 10^{-pH_2}, \quad (7)$$

where pH_1 and pH_2 are the average pH before and after the transition or complexation reaction.

During such processes, some of the protons are absorbed or released by the cacodylate buffer. The concentrations of these protons at 25°C, $\Delta[H^+]^{25}_{buf}$, were determined by combining the equations of equilibrium and mass balance for protonated and unprotonated forms of the buffer:

$$\Delta[H^+]^{25}_{buf} = C_T \frac{K_2 - K_1}{(1 + K_1)(1 + K_2)}. \quad (8)$$

C_T is the total buffer concentration (5 mM sodium cacodylate), K_2 is $10^{(pH_2 - pK_a)}$ and K_1 is $10^{(pH_1 - pK_a)}$. For cacodylate, the pK_a is 6.27 at 25°C; it changes only slightly with temperature. The total net change in the number of protons associated with DNA when it is perturbed is the sum of the net change of protons of the buffer and in solution:

$$\Delta[H^+]_{Tot} = \Delta[H^+]_{Soln} + \Delta[H^+]_{buf}. \quad (9)$$

RESULTS

Differential scanning calorimetry

The results of the heat capacity scans of the DNA-metal complexes are summarized in Table 1, which shows that all

TABLE 1 Thermodynamic and statistical parameters for the melting of DNA complexed with divalent metal cations*

Sample	T_m (°C)	ΔH_{cal} (kcal/mol bp)	ΔH_{vH} (kcal/mol bp)	$\langle n_{melt} \rangle$ (bp)	ΔS (cal/°K mol bp)	σ ($\times 10^3$)
DNA	75.5	6.7	75.6	11.3	19.3	10.9
MgDNA	83.6	7.8	145.5	18.7	21.9	4.6
CaDNA	79.2	8.7	163.7	18.8	24.7	4.1
SrDNA	83.5	7.3	135.8	18.6	20.6	4.6
BaDNA	81.2	6.2	129.6	20.9	17.5	3.5
MnDNA	77.2	8.6	100.5	11.7	24.5	10.3
CoDNA	67.8	7.3	184.4	25.3	21.4	2.2
NiDNA	62.5	6.7	188.6	28.1	19.9	1.9
CdDNA	51.8	6.8	102.3	15.0	21.0	5.8

*Samples contained 160 bp calf thymus DNA (55 mg/ml), 100 mM divalent metal chloride, and 5 mM sodium cacodylate (see Table 5 for pH).

of the alkaline earth and Mn complexes melt at higher temperatures than DNA without metal. This implies that the alkaline earths stabilize the DNA structure by reducing charge repulsion between the phosphates on each of the DNA strands. In contrast, the transition metals Co^{2+}, Ni^{2+}, and Cd^{2+} interact with the DNA bases, leading to disruption of the base pairs, destabilization of the DNA duplex, and a decrease in T_m. The melting curves are shown in Fig. 1. The order of effectiveness of the cations in affecting DNA melting is consistent with previous studies (Eichhorn and Shin, 1968) at similar metal/phosphate ratios.

ΔH_{cal} and ΔS_{cal} were determined to be 6.2–8.7 kcal/mol bp and 17.5–24.7 cal/K mol bp (Table 1). We attribute variations in these values to a combination of different binding affinities of the metals for the single- and double-stranded forms of DNA, and differences in hydration of the lyophilized DNA weighed out to prepare stock solutions under laboratory conditions of different humidity. However, all values are within the range of previous measurements of thermodynamic parameters for nucleic acid melting (Breslauer et al., 1986).

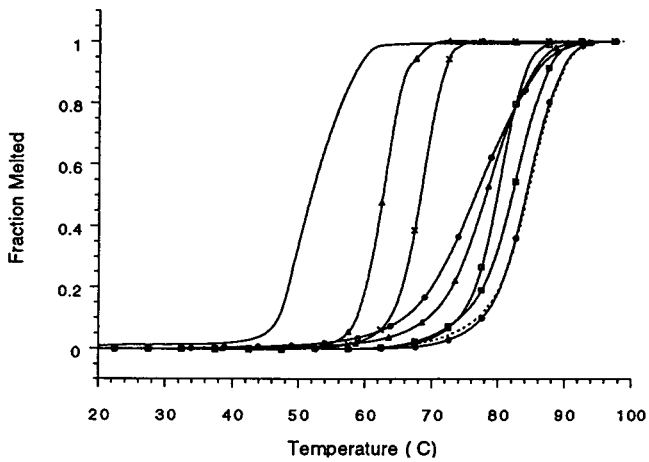

FIGURE 1 Fractional melting of DNA-metal complexes as determined by integrated heat capacity curves normalized between 0 and 1. Solutions contain 100 mM M^{2+}, 55 mg/ml DNA, and 5 mM sodium cacodylate. ——, CdDNA; ▲, NiDNA; ×, CoDNA; ○, DNA; △, MnDNA; □, CaDNA; ■, BaDNA; ●, MgDNA; - - - -, SrDNA.

The last column in Table 1 shows the apparent cooperativity parameter σ obtained by fitting the fractional melting from normalized integral heat capacity curves to helix-coil transition Eqs. 4–6. σ varies from 1.9×10^{-3} for NiDNA to 10.9×10^{-3} for DNA without metal. For homogeneous DNA, σ is related to the free energy of base stacking, ΔG_{BS}, by the equation

$$\sigma = \exp(\Delta G_{BS}/RT_m) \quad (10)$$

The values of σ and $\langle n_{melt} \rangle$ indicate a denaturation transition that is much broader than for homogeneous DNA (Crothers et al., 1964; Wada et al., 1980). This is due to the compositional heterogeneity of calf thymus DNA, which contains regions of base pairing that melt over a wide temperature range. Thus, under these circumstances, σ serves only as an empirical relationship to the free energy of base stacking.

Values of $\langle n_{melt} \rangle$ and σ in Table 1 also show that the cooperativity of melting is increased when enough divalent metal (100 mM) is available to neutralize all DNA phosphates (165 mM). Similar observations have been made for melting studies utilizing mono- and divalent cations (Dove and Davidson, 1962; Record, 1975). These results have been attributed to the fact that at low saturation of metal/DNA phosphate, partial denaturation releases bound cations, which become free to bind at other duplex sites. This results in increased stability of the unmelted regions and creates a broader melting transition, as we observe for DNA in the absence of metal. However, at high metal/DNA phosphate saturation, which is the condition for our DNA-metal complexes, the potential for metal interaction at available duplex sites is diminished during partial denaturation and the potential for transition broadening is thereby reduced.

Raman difference spectroscopy

Results from Raman difference spectroscopy of the DNA-metal complexes are shown in Figs. 2-8 and Tables 2 and 3. Complexes of CoDNA were not included in this study because absorption of laser radiation by the $CoCl_2$ solution resulted in heating and consequent deterioration of the sample. As in our previous study (Duguid et al., 1993), we were

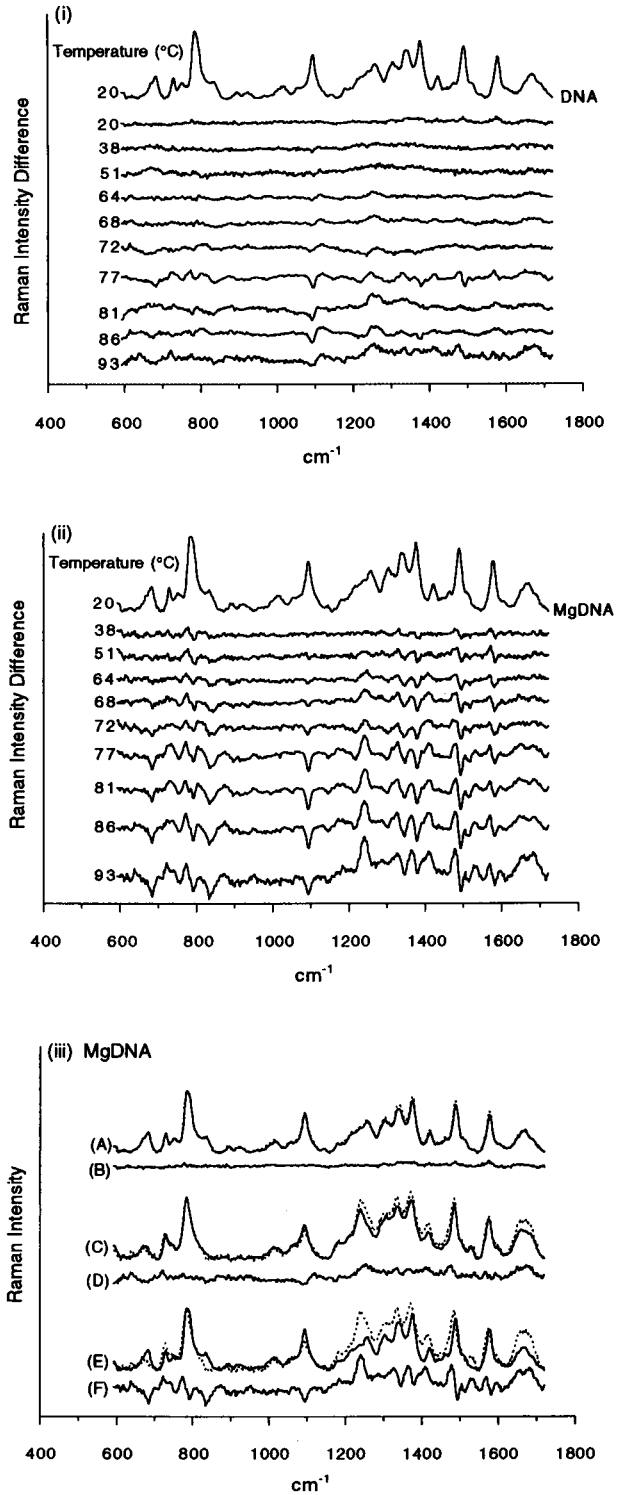

FIGURE 2 Raman difference spectra of 160 bp calf thymus MgDNA (100 mM Mg^{2+}, 55 mg/ml DNA) in aqueous buffer (5 mM sodium cacodylate). (*i*) Difference spectra [MgDNA (*T*)] − [DNA (*T*)] at the indicated temperature (*T*). (*ii*) Difference spectra [MgDNA (*T*)] − [MgDNA(20°C)]. (*iii*) (*A*) Superposition of the MgDNA spectrum (*dotted line*) on the DNA spectrum (*solid line*) at 20°C; (*B*) difference spectrum [MgDNA(20°C)] − [DNA(20°C)]; (*C*) superposition of the MgDNA spectrum (*dotted line*) on the DNA spectrum (*solid line*) at 93°C; (*D*) difference spectrum [MgDNA(93°)] − [DNA(93°)]; (*E*) superposition of the MgDNA spectrum at 93°C (*dotted line*) on the MgDNA spectrum at 20°C (*solid line*); (*F*) difference spectrum [MgDNA(93°C)] − [MgDNA(20°C)].

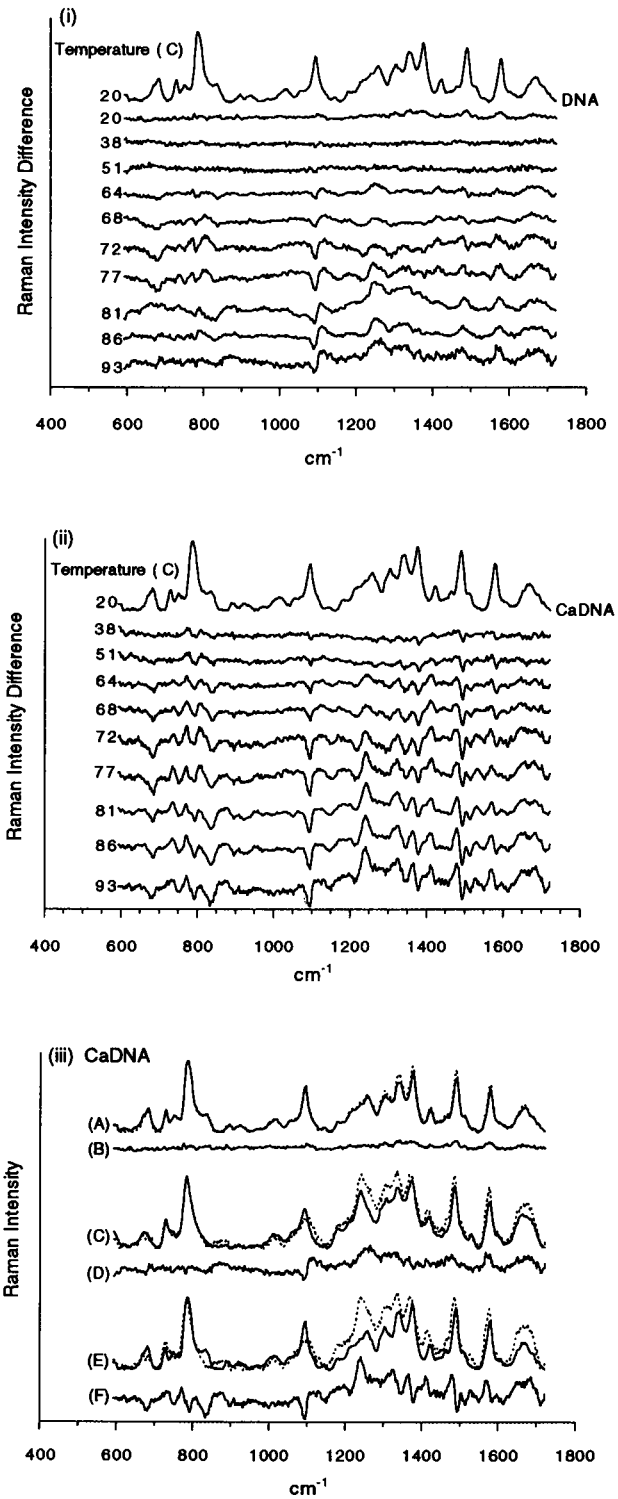

FIGURE 3 Raman difference spectra of 160 bp calf thymus CaDNA (100 mM Ca^{2+}, 55 mg/ml DNA) in aqueous buffer (5 mM sodium cacodylate). (*i*) Difference spectra [CaDNA (*T*)] − [DNA (*T*)] at the indicated temperature (*T*). (*ii*) Difference spectra [CaDNA (*T*)] − [CaDNA(20°C)]. (*iii*) (*A*) Superposition of the CaDNA spectrum (*dotted line*) on the DNA spectrum (*solid line*) at 20°C; (*B*) difference spectrum [CaDNA(20°C)] − [DNA(20°C)]; (*C*) superposition of the CaDNA spectrum (*dotted line*) on the DNA spectrum (*solid line*) at 93°C; (*D*) difference spectrum [CaDNA(93°)] − [DNA(93°)]; (*E*) superposition of the CaDNA spectrum at 93°C (*dotted line*) on the CaDNA spectrum at 20°C (*solid line*); (*F*) difference spectrum [CaDNA(93°C)] − [CaDNA(20°C)].

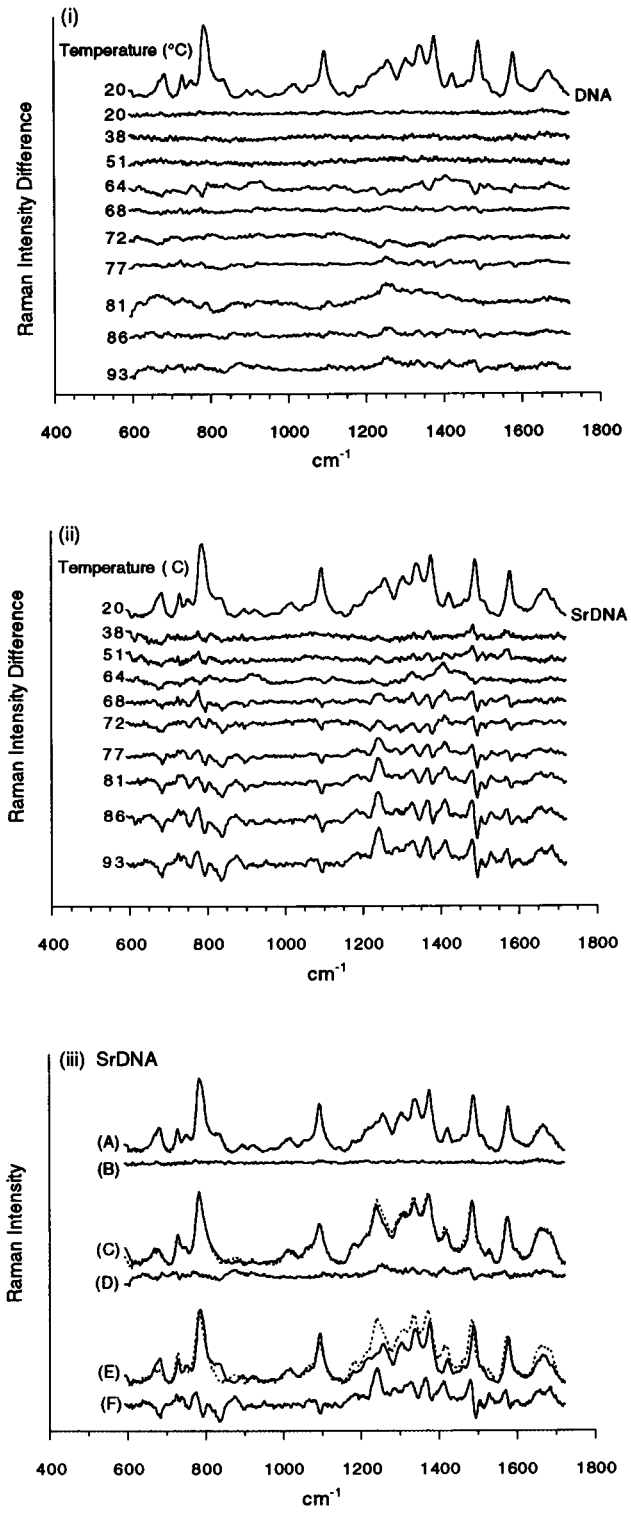

FIGURE 4 Raman difference spectra of 160 bp calf thymus SrDNA (100 mM Sr^{2+}, 55 mg/ml DNA) in aqueous buffer (5 mM sodium cacodylate). (*i*) Difference spectra [SrDNA (*T*)] − [DNA (*T*)] at the indicated temperature (*T*). (*ii*) Difference spectra [SrDNA (*T*)] − [SrDNA(20°C)]. (*iii*) (*A*) Superposition of the SrDNA spectrum (*dotted line*) on the DNA spectrum (*solid line*) at 20°C; (*B*) difference spectrum [SrDNA(20°C)] − [DNA(20°C)]; (*C*) superposition of the SrDNA spectrum (*dotted line*) on the DNA spectrum (*solid line*) at 93°C; (*D*) difference spectrum [SrDNA(93°)] − [DNA(93°)]; (*E*) superposition of the SrDNA spectrum at 93°C (*dotted line*) on the SrDNA spectrum at 20°C (*solid line*); (F) difference spectrum [SrDNA(93°C)] − [SrDNA(20°C)].

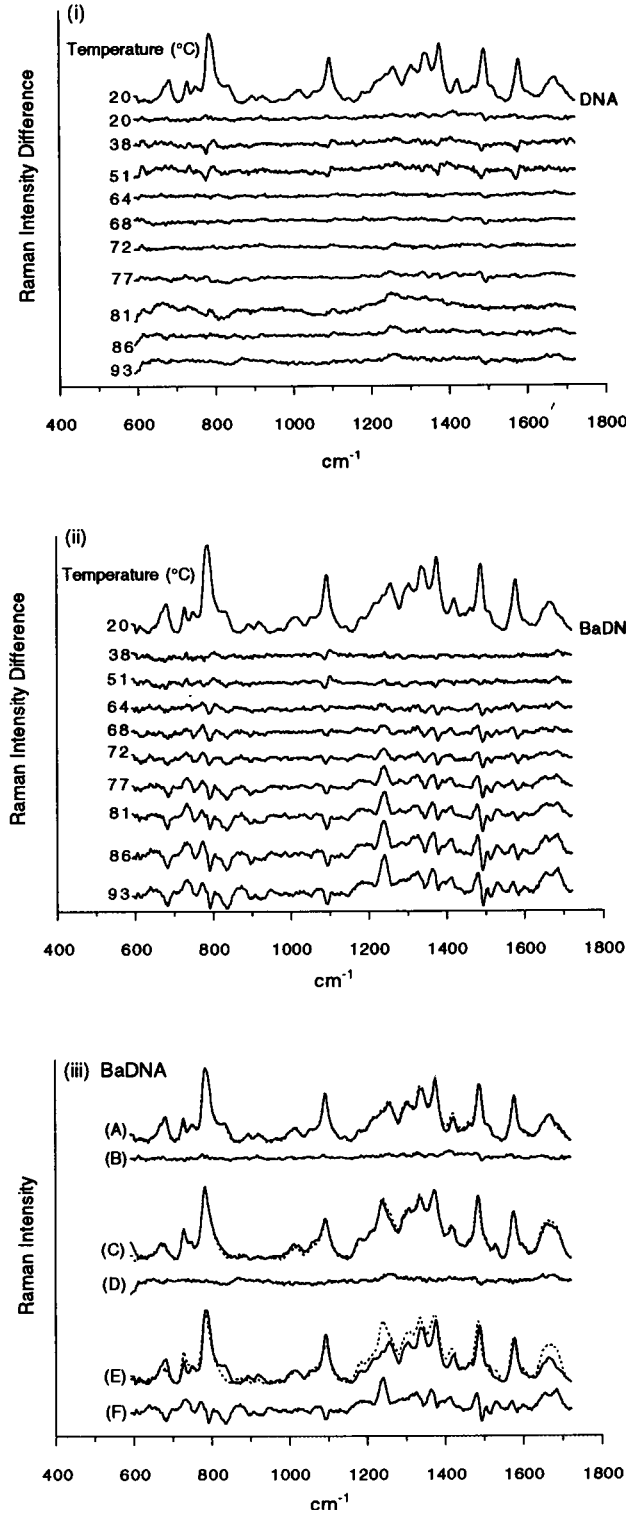

FIGURE 5 Raman difference spectra of 160 bp calf thymus BaDNA (100 mM Ba^{2+}, 55 mg/ml DNA) in aqueous buffer (5 mM sodium cacodylate). (*i*) Difference spectra [BaDNA (*T*)] − [DNA (*T*)] at the indicated temperature (*T*). (*ii*) Difference spectra [BaDNA (*T*)] − [BaDNA(20°C)]. (*iii*) (*A*) Superposition of the BaDNA spectrum (*dotted line*) on the DNA spectrum (*solid line*) at 20°C; (*B*) difference spectrum [BaDNA(20°C)] − [DNA(20°C)]; (*C*) superposition of the BaDNA spectrum (*dotted line*) on the DNA spectrum (*solid line*) at 93°C; (*D*) difference spectrum [BaDNA(93°)] − [DNA(93°)]; (*E*) superposition of the BaDNA spectrum at 93°C (*dotted line*) on the BaDNA spectrum at 20°C (*solid line*); (*F*) difference spectrum [BaDNA(93°C)] − [BaDNA(20°C)].

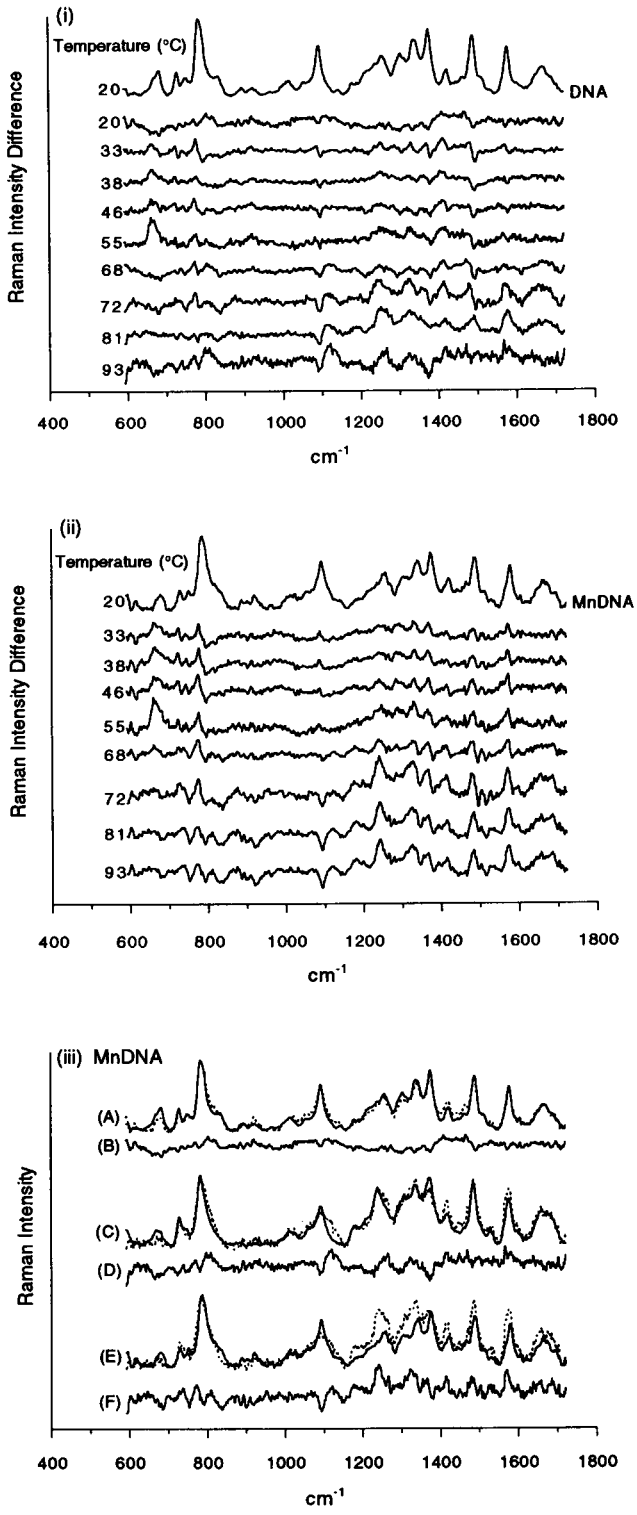

FIGURE 6 Raman difference spectra of 160 bp calf thymus MnDNA (100 mM Mn^{2+}, 55 mg/ml DNA) in aqueous buffer (5 mM sodium cacodylate). (*i*) Difference spectra [MnDNA (*T*)] − [DNA (*T*)] at the indicated temperature (*T*). (*ii*) Difference spectra [MnDNA (*T*)] − [MnDNA(20°C)]. (*iii*) (*A*) Superposition of the MnDNA spectrum (dotted) on the DNA spectrum (*solid line*) at 20°C; (*B*) difference spectrum [MnDNA(20°C)] − [DNA(20°C)]; (*C*) superposition of the MnDNA spectrum (*dotted line*) on the DNA spectrum (*solid line*) at 93°C; (*D*) difference spectrum [MnDNA(93°)] − [DNA(93°)]; (*E*) superposition of the MnDNA spectrum at 93°C (*dotted line*) on the MnDNA spectrum at 20°C (*solid line*); (*F*) difference spectrum [MnDNA(93°C)] − [MnDNA(20°C)].

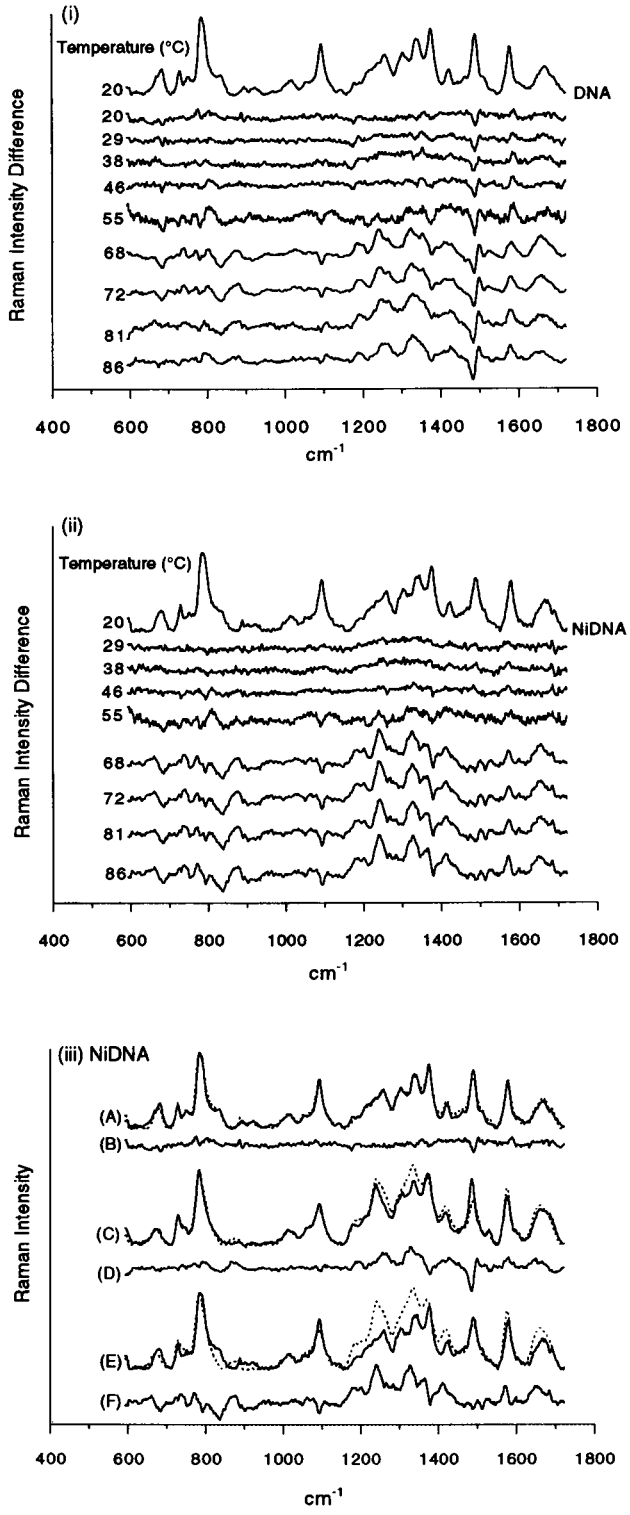

FIGURE 7 Raman difference spectra of 160 bp calf thymus NiDNA (100 mM Ni^{2+}, 55 mg/ml DNA) in aqueous buffer (5 mM sodium cacodylate). (*i*) Difference spectra [NiDNA (*T*)] − [DNA (*T*)] at the indicated temperature (*T*). (*ii*) Difference spectra [NiDNA (*T*)] − [NiDNA(20°C)]. (*iii*) (*A*) Superposition of the NiDNA spectrum (*dotted line*) on the DNA spectrum (*solid line*) at 20°C; (*B*) difference spectrum [NiDNA(20°C)] − [DNA(20°C)]; (*C*) superposition of the NiDNA spectrum (*dotted line*) on the DNA spectrum (*solid line*) at 93°C; (*D*) difference spectrum [NiDNA(93°)] − [DNA(93°)]; (*E*) superposition of the NiDNA spectrum at 93°C (*dotted line*) on the NiDNA spectrum at 20°C (*solid line*); (*F*) difference spectrum [NiDNA(93°C)] − [NiDNA(20°C)].

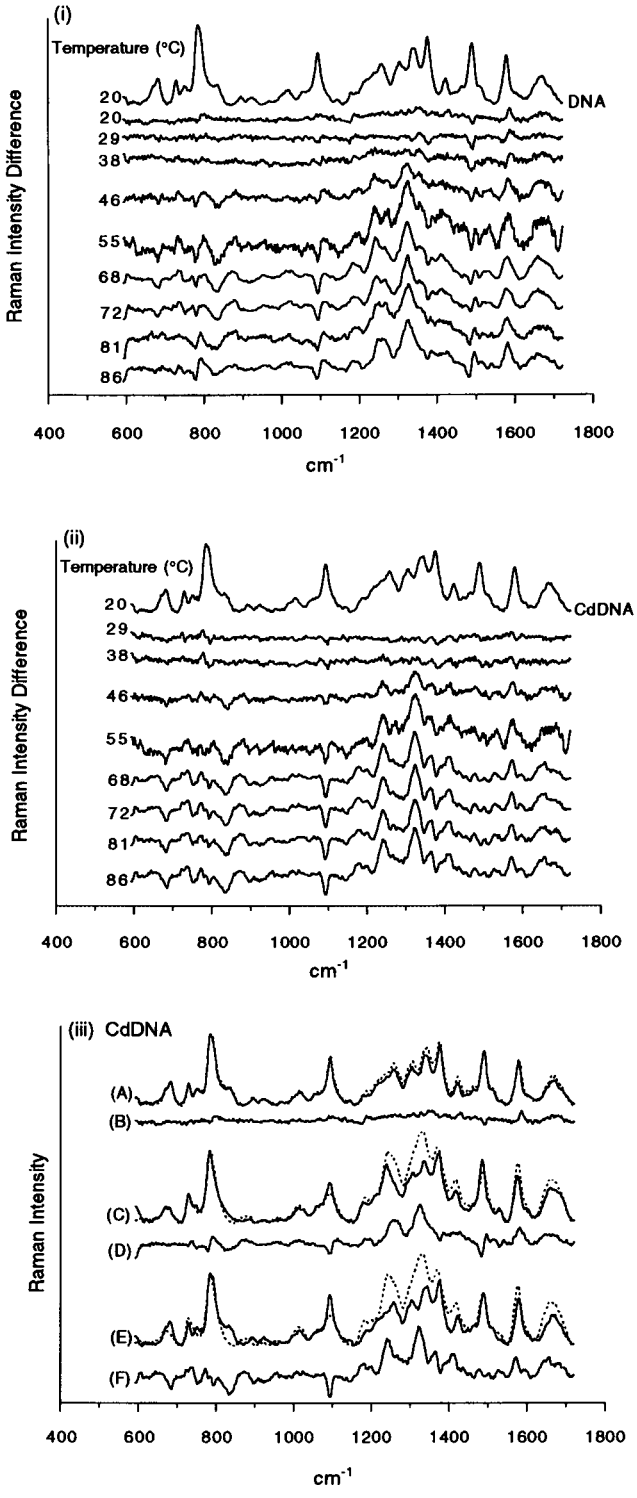

FIGURE 8 Raman difference spectra of 160 bp calf thymus CdDNA (100 mM Cd^{2+}, 55 mg/ml DNA) in aqueous buffer (5 mM sodium cacodylate). (*i*) Difference spectra [CdDNA (*T*)] − [DNA (*T*)] at the indicated temperature (*T*). (*ii*) Difference spectra [CdDNA (*T*)] − [CdDNA(20°C)]. (*iii*) (*A*) Superposition of the CdDNA spectrum (*dotted line*) on the DNA spectrum (*solid line*) at 20°C; (*B*) difference spectrum [CdDNA(20°C)] − [DNA(20°C)]; (*C*) superposition of the CdDNA spectrum (*dotted line*) on the DNA spectrum (*solid line*) at 93°C; (*D*) difference spectrum [CdDNA(93°)] − [DNA(93°)]; (*E*) superposition of the CdDNA spectrum at 93°C (*dotted line*) on the CdDNA spectrum at 20°C (*solid line*); (*F*) difference spectrum [CdDNA(93°C)] − [CdDNA(20°C)].

interested in the following spectra-structure correlations: a) The interval 620–685 cm^{-1} is responsive to glycosyl torsion and sugar puckering conformations of dG residues (Benevides et al., 1988; Thomas and Wang, 1988). b) The adenine marker near 729 cm^{-1} is sensitive to DNA melting but generally not to metal ion interactions (Thomas and Benevides, 1985; Thomas and Wang, 1988). c) The band near 750 cm^{-1} is sensitive to C2′-*endo/anti* conformers of dT residues (Thomas and Benevides, 1985). d) Bands from 800-1100 cm^{-1} are diagnostic of backbone geometry and secondary structure, especially the B form near 834 cm^{-1} (Benevides et al., 1991; Erfurth et al., 1972; Prescott et al., 1984; Tajmir-Riahi et al., 1988). e) At 1092 cm^{-1}, the PO_2^- marker is sensitive to hydration and strong electrostatic interactions of the phosphate group (Aubrey et al., 1992; Stangret and Savoie, 1992). f) From 1200–1600 cm^{-1}, various bands assigned to purine and pyrimidine vibrations are responsive to changes in the ring electronic structure and are sensitive to base unstacking, alterations in the local hydration, and metal binding at ring sites. These include the guanine band at 1489 cm^{-1}, which shifts to higher frequency with binding of electrophilic agents (H^+, metal ions, etc.) to the N7 acceptor (Moller et al., 1980), but increases in intensity and shifts to lower frequency during thermal denaturation of DNA in the absence of such agents (Duguid et al., 1993). The cytosine band near 1258 cm^{-1} (Benevides et al., 1991; Lord and Thomas, 1967) is highly sensitive to interactions between denatured DNA and divalent metal cations (Duguid et al., 1993), and the thymine band near 1240 cm^{-1} (Erfurth and Peticolas, 1975; Thomas and Benevides, 1985) is highly hypochromic in B-DNA and gains appreciable intensity with DNA denaturation (Erfurth and Peticolas, 1975). g) Centered near 1668 cm^{-1}, there is a broad band that is a superposition of several bands that are attributed to coupled C=O stretching and N-H deformation modes of dT, dG, and dC. This region is sensitive to hydrogen bonding states of the exocyclic donor and acceptor groups and shows a dramatic increase in intensity when DNA undergoes thermal denaturation (Benevides et al., 1991; Erfurth and Peticolas, 1975). There is also sensitivity of this region to deprotonation by metallation at N-H sites, which results in a decrease in intensity near 1680 cm^{-1} due to a shift to lower frequency of the C=O stretching and N-H deformation modes (Moller et al., 1980).

For each of the DNA-metal complexes, we present two types of Raman difference spectra, each obtained over the range 20–93°C: i) Subtraction of the spectrum of DNA without metal from that of the DNA-metal complex, both at the same temperature, shows metal-induced perturbations of the DNA before and after thermal denaturation/aggregation. ii) Subtraction of the spectrum of the DNA-metal complex at 20°C from that of the same complex at higher temperatures shows thermal perturbations of the complex. Comparison of the two types of difference spectra and their temperature dependence allows uncoupling of heat- and metal-induced effects on double- and single-stranded DNA.

TABLE 2 Metal effects that perturb the Raman spectrum of single-strand DNA: {DNA + M^{2+}, high temperature} + {DNA, high temperature}*

Marker bands Perturbed ν (cm^{-1})	MgDNA	CaDNA	SrDNA	BaDNA	MnDNA	NiDNA	CdDNA	Assignments†
681	—	−676, +685w	—	—	−663w	—	—	dG
729	—	—	—	—	—	—	—	dA
750	—		—	—	+736w	—	—	dT
781	—	—	—	—	+770, −783w	+795w	−778, +790m	dC
805	—	—	—	—	+804s	—	—	bk
834	—	−832vw	−833w	−834vw	−834vw	−839vw	−833w	bk(νOPO)
895	—	+870w	+872vw	+871vw	—	+871vw	+872vw	bk
1054	—	—	—	—	—	—	—	bk(νCO)
1092	−1089, +1115m	−1091, +1115s	—	—	−1092, +1113s	—	−1092, +1112m	bk(νPO_2^-)
1187	—	—	—	—	—	+1191w	+1190vw	dT, dC
1218	—	—	—	—	—	—	—	dT
1240	—	—	—	—	—	—	—	dT
1258	+1253m	+1256s	+1254w	+1258w	+1259s	+1260m	+1258s	dC, dA
1292	—	—	—	—	—	—	—	dC
1303	—	—	—	—	—	—	—	dA
1320	+1328w	+1321m	+1329w	—	+1327s	+1328s	+1325vs	dG
1335	—	—	—	—	—	—	—	dA, dG
1374	+1367w	+1364, −1378w	—	—	−1370m	+1356, −1378m	—	dT, dA, dG
1421	+1410w	+1410w	+1410w	—	+1415m	+1425w	—	δCH_2, dA
1489	+1476m	+1479m	+1476, −1492w	+1476, −1492w	—	−1483, +1498s	−1483, +1496s	dG, dA
1512	—	—	—	—	—	+1517vw	+1516vw	dA
1532	—	—	—	—	—	+1542vw	+1541vw	dC
1578	—	+1570m	—	—	+1575s	+1578w	+1582m	dG, dA
1602	—		—	—	—	—	—	dC
1668	+1649m, 1673m	+1649m, 1677m	—	+1672vw	—	+1649w	+1658w	νC=O, δNH_2 dT, dG, dC

*Raman intensities: vw, very weak; w, weak; m, medium; s, strong; vs, very strong; sh, shoulder. Plus and minus signs indicate peaks and lobes, respectively, in the difference spectrum.

†Bands assigned to nucleosides are indicated by dG, dA, dT, or dC. Other abbreviations: bk, backbone; νOPO, phosphodiester stretching mode; νCO, sugar C–O stretching mode; νPO_2^-, phosphodioxy stretching mode; δCH_2, methylene deformation mode; νC=O, carbonyl stretching mode; δNH_2, amino scissoring mode.

(I) Metal effects on dsDNA

The top panels (*i*) of Figs. 2–5 show that the alkaline earths do not alter the Raman spectra of duplex DNA below the melting temperature to any appreciable extent or in any consistent manner. This is different from the transition metals, which as shown in Figs. 6–8, interact with the N7 atom of purines and perturb the purine marker bands at 1489 and 1578 cm^{-1} (Duguid et al., 1993; Langlais et al., 1990; Mansy and Tobias, 1974; Moller et al., 1980). MnDNA (Fig. 6) shows additional peaks and lobes at 664, 724 (dA), and 773 (dC), 1092 (PO_2^-) and 1410 cm^{-1} (δCH_2, dA). These perturbations indicate unique metal-DNA interactions that are specific for Mn. The peak at 664 cm^{-1}, accompanied by the disappearance at 681 cm^{-1}, indicates a transition from the C2′-*endo/anti* to the C3′-*endo/anti* conformation of nucleosides associated with dG residues (Benevides et al., 1988; Thomas and Wang, 1988). Most other perturbations induced by DNA-metal complexes below the melting temperature are either weak or nonexistent. Thus, the major interactions with duplex DNA involve transition metals interacting at the N7 atom of guanine or between Mn and the DNA phosphates.

(II) Metal effects on ssDNA

Sugars

Most of the perturbations of the glycosyl torsions and nucleoside puckering are attributed to thermal effects and do not involve specific metal interactions. There is, however, a slight indication that Mn induces a weak decrease near 664 cm^{-1} as the dG nucleosides undergo a change from C3′-*endo/anti* to more random conformations at elevated temperatures.

Bases and exocyclic base residues

During denaturation of the DNA-metal complexes, the bands at 1240 cm^{-1} (dT) and 1258 cm^{-1} (dC, dA) increase in intensity, while the latter also shifts to higher frequency (~1264 cm^{-1}). The net effect of these perturbations is the formation of a single peak near 1258 cm^{-1} (Duguid et al., 1993) that is much greater in intensity relative to DNA without metal at the same temperature (Figs. 2–8, *i* and *iii*, and Table 2). A similar merger is observed for transition metals between bands at 1303 cm^{-1}, 1320 cm^{-1}, and 1335 cm^{-1}; this results in an unusually large peak near 1325

TABLE 3 Melting effects that perturb the Raman spectrum of metal-DNA complexes: {DNA + M^{2+}, high temperature} − {DNA + M^{2+}, low temperature}*

Marker bands Perturbed ν (cm^{-1})	DNA	MgDNA	CaDNA	SrDNA	BaDNA	MnDNA	NiDNA	CdDNA	Assignments†
681	−684m	−684m	−680w	−683m	−682m	−681w	+660, −684m	−684m	dG
729	+725w	+722sh	+722sh	+724sh	+723sh	+729sh	+726sh	+723sh	dA
750	+738w	+738, −757m	+734, −752m	+737, −755m	+732, −755m	+736, −752m	+736, −752m	+738, −750m	dT
781	+773, −792s	+773, −792s	+772, −792m	+773, −792s	+773, −791s	+770, −791m	+770, −793s	+772, −794m	dC
805	+803m	+810vw	+805vw	—	—	+808m	+805w	+805w	bk
834	−834m	−833s	−833s	−833m	−833m	−832m	−837m	−833s	bk(νOPO)
895	+872vw	+873vw	+871w	+873w	+870vw	—	+872m	+872m	bk
1054	+1060w	—	—	—	—	—	+1060vw	—	bk(νCO)
1092	−1092w	−1093m	−1095, +1120s	−1094w	−1093m	−1090, +1117s	+1093m	−1093s	bk(νPO_2^-)
1187	+1183w	+1183m	+1184m	+1184m	+1180m	+1179m	+1184m	+1180m	dT, dC
1218	—	—	+1197m	—	—	+1200w	+1201m	+1198m	dT
1240	+1240s	+1240vs	+1240vs	+1240s	+1240m	+1240s	+1239vs	+1240vs	dT
1258	—	—	+1264sh	—	—	+1264sh	+1266sh	+1264s	dC, dA
1292	+1289m	—	—	+1286s	—	—	—	—	dC
1303	+1308m	—	+1313sh	—	—	—	—	—	dA
1320	—	—	—	—	—	+1323s	+1326vs	+1322vs	dG
1335	+1324, −1343m	+1326, −1346s	+1324, −1347s	+1326, −1346m	+1325, −1342m	—	—	—	dA, dG
1374	+1363, −1381s	+1363, −1381s	+1366, −1378s	+1365, −1381s	+1363, −1378m	+1363, −1381	+1364, −1379s	+1364, −1378s	dT, dA, dG
1421	+1412m	+1413s	+1410s	+1410s	+1413m	+1412w	+1410s	+1410s	δCH_2, dA
1489	+1481, −1494s	+1478, 1493vs	+1479, 1492vs	+1479, −1494vs	+1480, −1492s	+1480s	+1474vw	+1476w	dG, dA
1512	+1504vw	+1505w	+1502w	+1504vw	+1505vw	+1501w	+1500vw	+1502vw	dA
1532	+1528m	+1531m	+1526m	+1528m	+1529w	+1528vw	+1527vw	+1527w	dC
1578	+1572, −1582m	+1569, −1582s	+1568s	+1569, −1582m	+1571, −1583m	+1571s	+1571m	+1572m	dG, dA
1602	+1597vw	+1596w	+1596w	+1596vw	+1598vw	+1598w	+1599vw	+1597w	dC
1668	+1654m, +1684m	+1658s, +1681s	+1656s, +1682s	+1658m, +1684m	+1654m, +1684s	+1656s, +1683s	+1657m, +1680m	+1657s, +1680m	νC=O, δNH_2 dT, dG, dC

*Raman intensities: vw, very weak; w, weak; m, medium; s, strong; vs, very strong; sh, shoulder. Plus and minus signs indicate peaks and lobes, respectively, in the difference spectrum.
†See Table 2.

cm^{-1} in both temperature- and metal-dependent difference spectra (Figs. 6–8, Table 2). Similar observations are made for alkaline earth-ssDNA complexes, but are much weaker.

Raman difference spectra comparing ssDNA-metal complexes with DNA in the absence of metal show that melting is more extensive in the presence of metals. This is observed in the form of qualitatively similar, but greater, perturbations at 1374, 1421, 1532, 1578, and 1668 cm^{-1}, the latter of which shows a more extensive band shift toward lower frequencies. The enhanced melting of these complexes may be related to the increased cooperativity effect induced by the divalent metals.

Different changes occur for some of the ring base vibrations, depending on whether the perturbation is due to thermal melting or metal ion interaction. The band at 781 cm^{-1} (dC) shifts to lower frequency upon thermal denaturation of DNA (Duguid et al., in preparation), but to higher frequency when there are metals present that bind to N3 atoms of pyrimidine bases (Mansy and Tobias, 1974; Moller et al., 1980). Table 2 shows that the shifts to higher frequency are only observed for the transition metals Cd^{2+} and Ni^{2+}, the former having a stronger effect than the latter. Similarly, during thermal denaturation of DNA in the absence of metal, a shift to lower frequency and an increase in intensity are observed in the difference spectra near 1489 cm^{-1} (Duguid et al., in preparation). Parts *i* and *iii* of Figs. 7 and 8 show that this band shifts toward higher frequency and remains hypochromic when Cd^{2+} and Ni^{2+} are bound to ssDNA. Similar frequency shifts have been observed upon heavy metal binding to guanine residues (Mansy et al., 1978; Moller et al., 1980). No such effects are observed for alkaline earth-ssDNA complexes, which indicates less reactivity, relative to Cd^{2+} and Ni^{2+}, for the purine bases of ssDNA. These two cases indicate that Cd and Ni react readily with the N3 atom of cytosine and with the N7 atom of purines. Based on previous observations, the latter interaction is most likely with guanine.

Backbone

Compared with the base vibrations, metal interactions with thermally denatured DNA induce qualitatively similar, but quantitatively larger melting effects. Most of the complexes show a lower intensity at 834 cm^{-1}, a higher intensity near 872 cm^{-1}, and greater perturbations at 1092 cm^{-1}, than observed for DNA melting in the absence of metal.

Interestingly, the phosphodioxy band at 1092 cm^{-1} decreases in intensity and shifts to higher frequency when ssDNA-metal complexes are compared to those of ssDNA in the absence of metal (Figs. 2–8, *i*). Similar perturbations have been observed upon metal binding to ionic phosphates of DNA (Aubrey et al., 1992; Lord and Thomas, 1968) and of polyphosphate (Stangret and Savoie, 1992). We interpret this effect as resulting from disruption of the hydrogen bonds between the phosphate oxygens and hydrogens of water, coupled to metal interactions with the newly exposed phosphates. This interpretation is consistent with previous assessments based on IR spectra of phosphate compounds

(Shimanouchi et al., 1964), and with Raman studies of phosphate-divalent metal interactions (Aubrey et al., 1992; Brown and Peticolas, 1975; Lord and Thomas, 1968; Stangret and Savoie, 1992).

(III) Melting effects

Most of the thermal perturbations of the DNA-metal complexes are similar, and for most bands, thermal denaturation behavior resembles that of DNA in the absence of metal, especially for the alkaline earth-DNA complexes. Except where there are notable differences, we will generalize most of the thermal effects on the difference spectra of the DNA-metal complexes, which are illustrated in parts *ii* and *iii* of Figs. 2–8 and summarized in Table 3.

Sugars

As torsional rotations about the glycosyl bonds become more flexible during thermal denaturation, characteristic changes occur at 681 cm^{-1} (dG) and 750 cm^{-1} (dT). For all DNA-metal complexes, a decrease in intensity is observed near 681 cm^{-1}, whereas the thymidine band near 750 cm^{-1} broadens and shifts to a lower frequency (~735 cm^{-1}). In duplex DNA, the 681 cm^{-1} band normally identifies C2′-*endo/anti* conformations of sugars linked to guanine residues, whereas a shift to 664 cm^{-1} is diagnostic of the appearance of C3′-*endo/anti* conformers (Benevides et al., 1988; Thomas and Wang, 1988). Similarly, the marker near 750 cm^{-1} identifies C2′-*endo/anti* conformers of dT (Thomas and Benevides, 1985).

Bases and exocyclic base residues

Changes upon melting in the spectral regions of base vibrations around 600–800 cm^{-1} are similar for all the DNA-metal complexes and for DNA without metal. The purine ring breathing vibration of adenine at 729 cm^{-1} (Thomas and Benevides, 1985; Thomas and Wang, 1988) increases in intensity and shifts to a lower frequency as the bases become unstacked, whereas the cytosine marker (781 cm^{-1}) shifts to lower frequency. The increase in Raman intensity that often occurs when DNA bases become unstacked is attributed to removal of the attenuation (hypochromic effect) due to nearest-neighbor interactions between ring breathing vibrations.

In the region 1180–1600 cm^{-1}, there are many perturbations in the Raman difference spectra that occur during thermal denaturation, which are similar for all DNA-metal complexes and for DNA without metal. The major frequencies where similar modifications occur include 1187 (dT, dC), 1240 (dT), 1374 (dT, dA, dG), 1421 (δCH_2, dA), 1512 (dA), 1532 (dC), and 1602 cm^{-1}(dC). Several of these bands, particularly at 1187 cm^{-1} and 1240 cm^{-1}, increase significantly in intensity during thermal denaturation. These increases are attributed to removal of the attenuation exerted by stacked bases on their nearest neighbors as the DNA melts (Duguid et al., in preparation; Erfurth and Peticolas, 1975).

There are, however, several spectral modifications between 1180 and 1600 cm^{-1} that distinguish alkaline earth from transition metal complexes during thermal denaturation. For transition metal-DNA complexes, a merger is observed between the two hyperchromic bands at 1187 cm^{-1} and 1218 cm^{-1}, brought about by the shift to lower frequency of the latter. This shift is most likely due to a decrease in electron delocalization in the thymine base as the DNA melts and the metal ions interact with the melted structure.

In the region 1300–1600 cm^{-1}, many bands shift to lower frequency during thermal denaturation of alkaline earth-DNA complexes. Most of these bands are dominated by vibrations from purine residues and include bands near 1335 cm^{-1} (dA, dG), 1374 cm^{-1} (dT, dA, dG), 1489 cm^{-1} (dA, dG), and 1578 cm^{-1} (dA, dG). One explanation for these concerted frequency shifts may be that as the temperature is raised and the DNA-metal complexes denature, hydrogen bonds are ruptured between the DNA and the solvent. The result is a decrease in frequency of all base vibrations that are sensitive to this "dehydration" effect. Another possibility is that some of these vibrations are sensitive to different hydrogen bonding environments and that trading base-base hydrogen bonds for base-water hydrogen bonds during thermal denaturation might lower the frequency.

Near 1325 cm^{-1}, there is a major difference between thermally induced perturbations of alkaline earth- and transition metal-DNA complexes. The former results from a shift to lower frequency of the purine ring vibrations near 1335 cm^{-1}, whereas the latter has an additional contribution from a large, broad-intensity increase of the band at 1320 cm^{-1}, assigned to dG residues. This latter effect can be ascribed to differences in transition metal perturbations between double- and single-stranded DNA. Interestingly, in this spectral region, melting profiles for CaDNA and MnDNA are intermediate between those of other alkaline earth and transition metal complexes. Fig. 9 and Table 4 show that this effect can be observed quantitatively by monitoring the ratio I_{1335}/I_{1374}, which increases in the order DNA < Sr < Ba < Mg < Ca < Mn < Ni < Cd.

Other thermal perturbations that distinguish alkaline earth from transition metal-DNA complexes occur at 1489 cm^{-1} and 1578 cm^{-1}. For alkaline earth complexes, these bands tend to increase in intensity and shift to a lower frequency during thermal denaturation. In the presence of transition metals, these perturbations are offset at 1489 cm^{-1} by metal binding to the N7 atom of guanine, whose spectral signature opposes that of thermally induced melting. To a much lesser extent, similar comparisons can be made of the influence of the two classes of metals on the 1578 cm^{-1} band, which is also a marker for purine residues.

The broad band centered near 1668 cm^{-1} contains contributions from both C=O stretching and N-H deformation

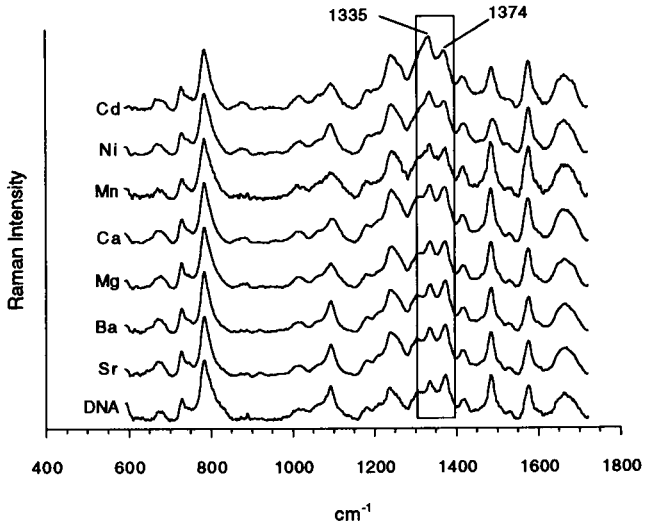

FIGURE 9 Raman spectra of DNA and DNA-metal complexes obtained at 81°C, showing intensities of bands at 1335 and 1374 cm^{-1}. Each spectrum is normalized to the intensity of the band at 786 cm^{-1}.

modes of dT, dG, and dC (Erfurth and Peticolas, 1975). Figs. 2–8 *ii* show that the intensities increase in this region during thermal denaturation of all DNA-metal complexes, with difference spectral maxima near 1657 and 1680 cm^{-1}. Comparisons with previous studies indicate that these maxima are hyperchromicities associated, respectively, with the C4═O and C2═O stretching vibrations of thymine (Erfurth and Peticolas, 1975; Lafleur et al., 1972; Small and Peticolas, 1971).

Backbone

The phosphodiester band at 834 cm^{-1} decreases in intensity and broadens for all DNA-metal complexes as the DNA backbone becomes more flexible during thermal denaturation (Erfurth et al., 1972; Prescott et al., 1984). This effect occurs for most backbone vibrations and can be observed throughout the region 800-1050 cm^{-1}. The melting perturbations within this region are qualitatively similar for all DNA-metal complexes and for DNA in the absence of metal (i.e., intensity decreases at 895 and 923 cm^{-1} and increases near 805 and 872 cm^{-1}).

The phosphodioxy band at 1092 cm^{-1} decreases in intensity as the DNA-metal complexes melt; in some cases, it also shifts to higher frequency (Figs. 2–8, *ii*). These effects were also observed in the difference spectra between ssDNA-metal complexes and ssDNA in the absence of metal. Such similarities between the two types of difference spectra indicate coupling between the thermal and metal binding effects on PO_2^- stretch vibrations.

TABLE 4 Correlation of I_{1335}/I_{1374} with the midpoint of DNA aggregation (T_a) and melting (T_m)*

Sample	I_{1335}/I_{1374}	T_a	T_m
DNA	0.86	—	75.5
BaDNA	0.92	—	81.2
SrDNA	0.93	—	83.5
MgDNA	1.01	84.9	83.6
CaDNA	1.04	76.4	79.2
MnDNA	1.07	76.7†	77.2
CoDNA	—	60.3	67.8
NiDNA	1.18	58.3	62.5
CdDNA	1.24	55.4	51.8

*Solutions contained 160 bp mononucleosomal calf thymus DNA (55 mg/ml), 100 mM divalent metal chloride, and 5 mM sodium cacodylate. The pH of the sodium cacodylate buffer was originally 6.47.
†Because MnDNA does not disaggregate, T_a is an estimate from theoretical calculations.

(iv) Raman signatures of DNA melting

Previous studies (Duguid et al., in preparation; Erfurth and Peticolas, 1975; Rimai et al., 1974) have utilized intensity changes of several Raman bands to monitor thermal melting of DNA. One of the most common features is the decrease in intensity of the phosphodiester backbone vibration at 834 cm^{-1}, which signifies a reduction of DNA backbone order. Traditionally, intensity increases at 1240 cm^{-1} (dT) and 1668 cm^{-1} ($\nu C{=}O$, δNH_2) have been diagnostic indicators of base stacking and base pairing, both of which are perturbed during DNA melting. Unfortunately, the use of intensity changes of base marker bands to monitor DNA melting in the presence of divalent cations is complicated by the base-metal interactions, which tend to offset the intensity increases normally observed. In addition, the differential affinities of the metal-base interactions at different temperatures result in difficulties in establishing adequate baselines for the base marker bands to be used as a quantitative measure of DNA melting or aggregation. Still, as seen in Figs. 2–8, it is clear that significant intensity increases of the base marker bands have occurred after the melting/aggregation transition, indicative of base unstacking and base-pair disruption.

The most reliable indicator of DNA denaturation/aggregation is the backbone marker at 834 cm^{-1}, which tends to be less affected by direct metal interactions. Nonetheless, as shown by some representative plots in Fig. 10, there are some difficulties in establishing a well-defined baseline for quantitating thermal melting/aggregation profiles. In general we can state that after DNA aggregation and thermal denaturation, the intensities of phosphate backbone bands at 834 cm^{-1} and 1092 cm^{-1} decrease as the temperature is raised, whereas the intensities of the base ring vibrations at 1187, 1240, 1335, 1421, and 1668 cm^{-1} increase. All of these factors reveal backbone disorder and base unstacking during DNA denaturation (Erfurth and Peticolas, 1975).

(v) Structure of melted Ni and Cd complexes

Several features of the Raman spectra of melted forms of NiDNA and CdDNA are characteristic of C-DNA (Erfurth et al., 1972; O'Connor et al., 1982). These include a shift to

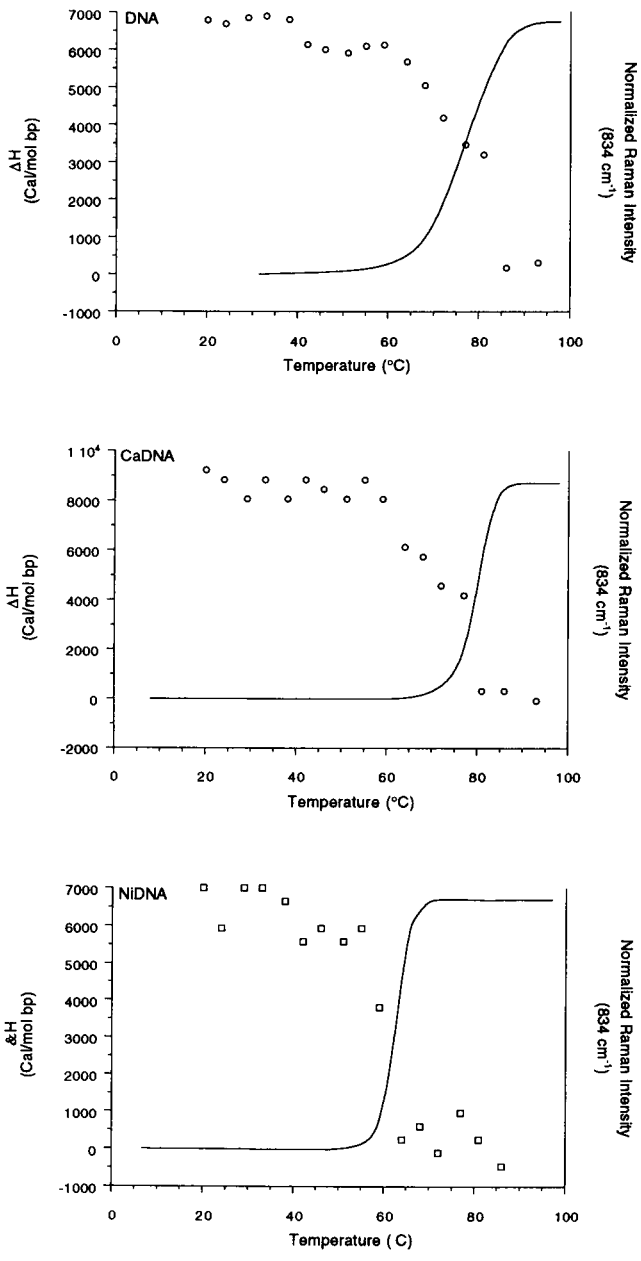

FIGURE 10 Plots of the integrated heat capacity of DNA (*top*), CaDNA (*middle*), and NiDNA (*bottom*) versus the intensity of the Raman marker at 834 cm^{-1} (*open symbols*).

lower frequency of the 681 cm^{-1} and 750 cm^{-1} bands, the appearance of a band at 872 cm^{-1}, and enhanced intensity near the 1325 cm^{-1} band relative to other ring vibrations in this region. Whereas the first three perturbations are also seen for DNA melting, the last one is unique to C-DNA (Erfurth et al., 1972). The spectral region between 1187 and 1374 cm^{-1} also displays relative intensities of the base ring bands that are similar those of C-DNA. Although NiDNA and CdDNA contain all of the features that are characteristic of thermally denatured DNA (decreased backbone order, base unstacking, and base-pair disruption), the secondary structure deduced from Raman spectroscopy is different from that for melted DNA in the absence of metal. No similarities could be identified between the DNA-metal complexes and any other DNA secondary structures (A, Z, etc.) at any other temperatures.

Optical densitometry and aggregation

As most of the DNA-metal complexes are heated in solution, they become increasingly turbid. The turbidity reaches a maximum, then subsides. This is presumably due to DNA aggregation, and subsequent dissolution of the aggregate as ssDNA forms. Representative plots of this turbidity profile are shown in Fig. 11. Fig. 12 shows the integral curves of the observed turbidity, normalized between 0 and 1 to indicate the extent of the aggregation transition for each of the DNA-metal complexes. Inspection of the transition metal-DNA complexes after cooling to room temperature reveals that they have formed a gel. There was no measurable turbidity for SrDNA, BaDNA, or DNA without metal.

The behavior of peaks in the Raman spectrum at 1335 cm^{-1} and 1374 cm^{-1}, shown in Fig. 9, provides a striking correlation with the ability of DNA-metal complexes to aggregate at elevated temperatures. Comparison in Table 4 of the intensity ratio I_{1335}/I_{1374} with the temperature for the midpoint of aggregation, T_a, shows that aggregation will occur if I_{1335}/I_{1374} is greater than 1. Higher ratios give lower T_a and T_m. DNA, SrDNA, and BaDNA ($I_{1335}/I_{1374} < 1$) do not show measurable aggregation. At the other extreme, Ni and CdDNA ($I_{1335}/I_{1374} > 1$) aggregate appreciably and have low T_m values. Mg, Ca, and MnDNA ($I_{1335}/I_{1374} \geq 1$) are intermediate. This correlation suggests that perturbation of the bases, especially the purines, is associated with aggregation. Table 4 shows that the midpoint of DNA aggregation (T_a) occurs at temperatures that are near or slightly below T_m. Fig. 13 shows the strong correlation between T_a and T_m for different DNA-metal complexes, implying that the mechanisms of aggregation and denaturation are closely related.

pH potentiometry

Results from pH potentiometry are shown in Table 5. The pH drops when divalent cations are added to DNA, in the order Cd > Ni > Co > Mn > Ca > Mg > Sr > Ba at room temperature. The pH drop is small but systematically larger in the presence of transition metal cations. The concentration of protons displaced during DNA-metal mixing ($\Delta[H^+]^{25°C}_{Mix}$) is about 2.4–3.13 mM, most of which is absorbed by the cacodylate buffer, in a solution that is 165 mM in DNA-phosphate. The only protonated sites on double-stranded DNA that can be displaced by Ni^{2+} or Cd^{2+} within the pH range 3.9 to 6.5 are terminal phosphates, which are present at 2 mM concentration. These phosphates do not fully account for the total concentration of displaced protons. Assignments of displacement at other protonated sites cannot be unambiguously made. Although proton dis-

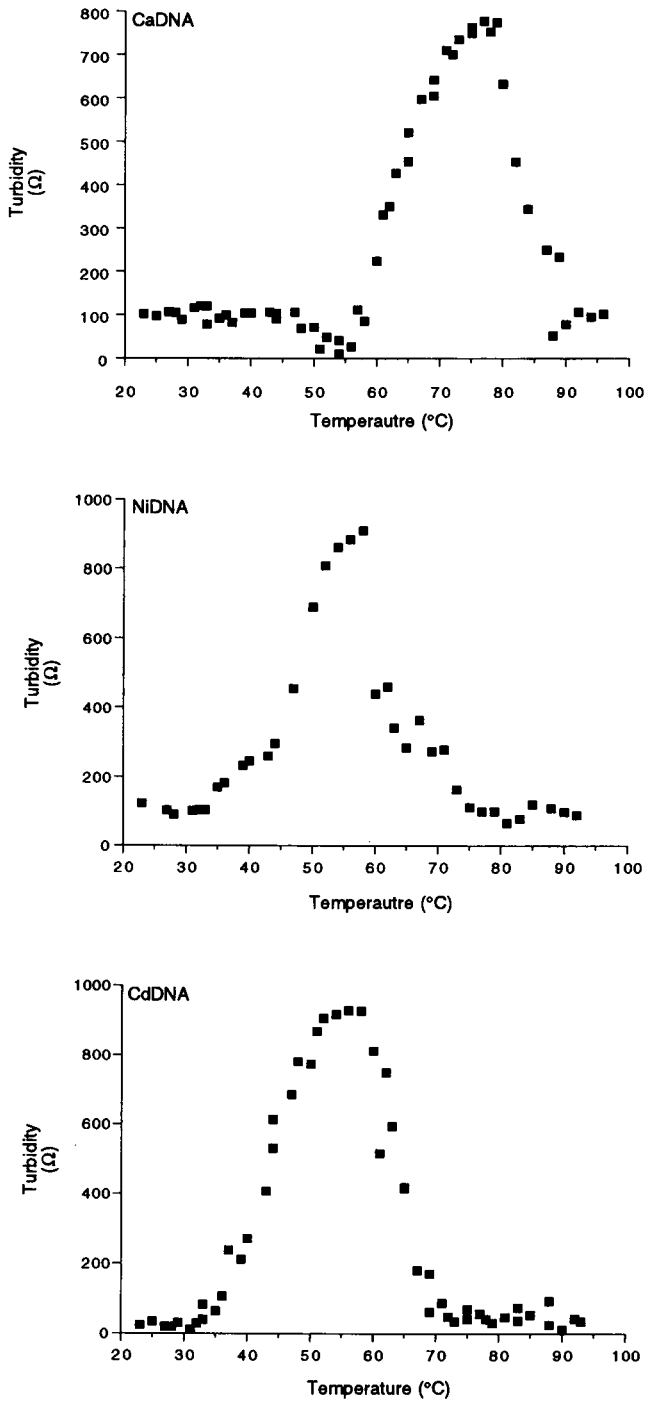

FIGURE 11 Turbidity profiles measured as a function of resistance (Ω) versus temperature (°C) for representative complexes of DNA with Ca, Ni, and Cd.

placement at terminal phosphates is a possibility, it is also possible that most of the source of deprotonation comes from base NH or NH_2 groups upon metal complexation. In such a scenario, proton release might be another manifestation of titratable joints, induced by either covalently or noncovalently bound polyamines (Wilcoxon et al., 1984).

Fig. 14 compares the temperature-dependent profiles of pH, aggregation, and melting for representative samples of

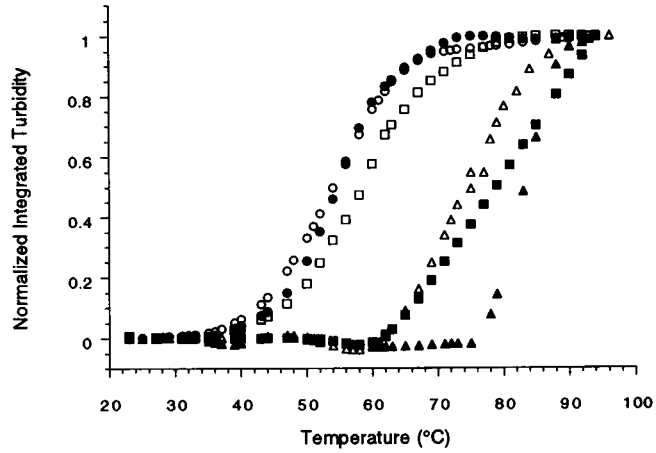

FIGURE 12 Normalized integrated turbidity profiles of DNA-metal complexes. ○, CdDNA; ●, NiDNA; □, CoDNA; ■, MnDNA; △, CaDNA; ▲, MgDNA.

the DNA-metal complexes. The pH of the MgDNA solution decreases steadily before aggregation and melting. Similar effects are seen for SrDNA and BaDNA. It appears that although Sr^{2+}, Ba^{2+}, and Mg^{2+} do not induce deprotonation as extensively as the other divalent cations (Table 5), they do render these proton sites labile to heating.

The pH of solutions containing the DNA-metal complexes increases during aggregation, until the complex is completely melted. This indicates that during the transition, protons are removed from solution through binding to newly exposed base sites. These sites (N1 atom of adenine and N3 atom of cytosine) have pK_a values that are above the solution pH of the DNA-metal complex and can act as buffering agents. The pH of the solution at the higher end of the temperature range tends to level off near the pK_a values of these base sites (~4.4–5.0). When the aggregation curve is superimposable on the melting curve (MgDNA), or when there is no measurable aggregate formation (SrDNA and BaDNA), the pH increase coincides with the melting tran-

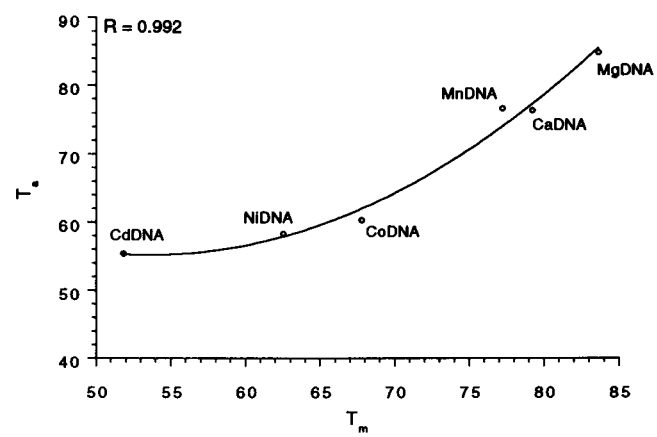

FIGURE 13 Correlation analysis between the melting temperature (T_m) and the aggregation temperature (T_a) of different DNA-metal complexes.

TABLE 5 pH changes upon metal-DNA complexation*

Control	pH	Solutions	pH	DNA	$pH_{25°C}$	pH_{melt}	$\Delta[H^+]^{25°C}_{Mix}$ (mM)	$\Delta[H^+]^{Melt}_{Tot}$ (μM)
Buffer	6.47	$SrCl_2$	6.37	SrDNA	4.79	4.91	2.63	134†
DNA	6.36	$BaCl_2$	6.37	BaDNA	5.14	4.95	2.43	34.6†
		$MgCl_2$	6.37	MgDNA	4.73	4.81	2.65	140†
		$CaCl_2$	6.37	CaDNA	4.15	4.76	2.80	166
		$MnCl_2$	6.37	MnDNA	4.11	5.05	2.82	319
		$CoCl_2$	6.13	CoDNA	3.92	4.75	2.48	227
		$NiCl_2$	6.30	NiDNA	3.93	4.6	2.76	174
		$CdCl_2$	6.58	CdDNA	3.91	4.56	3.13	169

*Solutions contained 160 bp mononucleosomal calf thymus DNA (55 mg/ml), 100 mM divalent metal chloride, and 5 mM sodium cacodylate. The pH of the sodium cacodylate buffer was originally 6.47.

†Because of a pH drop at elevated temperatures, $\Delta[H^+]^{melt}_{tot}$ was calculated using as a reference pH values at temperatures slightly below the onset of melting instead of the pH at 25°C. These reference pH values are 4.54 (SrDNA), 4.88 (BaDNA), and 4.34 (MgDNA).

sition. By applying Eqs. 7–9 to the pH differences between the melted and unmelted metal-DNA complexes, the concentration of protons absorbed by these DNA-metal complexes during aggregation and denaturation ($\Delta[H^+]^{Melt}{}_{Tot}$) was estimated to be in the range 34–320 μM (Table 5). No pH change was observed during thermal denaturation of DNA in the absence of metal.

DISCUSSION

Information from a variety of techniques allows us to construct a fairly detailed picture of events taking place when divalent metal cations are added to DNA and the solutions are heated. It should be borne in mind that these solutions are quite concentrated: about 165 mM DNA-P and 100 mM divalent metal ion. They are intended not to mimic physiological conditions, but rather to explore the structural and chemical changes provoked by forcing conditions.

At room temperature, the DNA remains in the B-conformation, and Raman spectroscopy shows no signs of interaction with the alkaline earth ions, whereas both Ni^{2+} and Cd^{2+} bind to the N7 acceptor of guanine in dsDNA. The interaction of this site is stronger with Ni^{2+}, as indicated by larger perturbations at 1489 cm^{-1} (compare Figs. 7 and 8). Potentiometry reveals a drop in pH, ranging from 1.2 units for BaDNA to 2.2 units for CaDNA, that betokens some interaction between the bases and alkaline earths. Most of the protons are probably displaced from the terminal phosphates, but this cannot be conclusively demonstrated. Deprotonation is probably not observed spectroscopically, because it occurs at only a small fraction of the protonated sites on the DNA. Sr, Ba, and Mg, but not Ca, cause additional proton displacement as the temperature is raised but before the onset of the melting transition. This implies a labilization of base protons by these ions.

During aggregation and/or thermal denaturation, the pH increases, suggesting that protons bind to newly exposed base sites. Because the pH of solutions of metal-melted DNA complexes is between 4.5 and 5.0, we suggest that the N1 atoms of adenine and/or the N3 atoms of cytosine act as buffering sites once they become exposed. Interactions of Ni^{2+} and Cd^{2+}, and/or protons, with the N3 atom of cytosine are observed in ssDNA, as indicated by perturbations at 781 cm^{-1}.

Although the differences are slight, the transition metals, which are considered to be more mutagenic than the alkaline earths, induce greater proton displacement from the DNA. In addition, there is evidence (Kasprzak and Waalkes, 1986) that Ca^{2+}, which causes greater deprotonation than other alkaline earths, can enhance chemical carcinogenesis, although the exact mechanism is unknown. These observations raise the possibility that divalent cations may induce acid-catalyzed activation of certain mutagens through displacement of protons from the DNA. Fig. 15 shows one possible mechanism in which protons are displaced by divalent cations, resulting in the activation of another mutagen that can form an adduct with DNA. The free protons in solution, created by the metal-DNA interactions, contribute to an already low pH in the immediate vicinity of DNA, as indicated by Poisson-Boltzmann calculations of counterion distributions (Lamm and Pack, 1990). The combination of these two effects could strongly enhance the action of mutagens that require acid catalysis for activation. This idea will require further study.

As the DNA-metal complexes melt, there are noteworthy variations in the Raman spectra between 1300 and 1400 cm^{-1}, especially the intensity changes at 1335 and 1374 cm^{-1}. The ratio I_{1335}/I_{1374} correlates with the capacity of the DNA-metal complexes to form aggregates. This suggests that DNA aggregation is related in some way to changes in vibrations of the bases, a not surprising relation if aggregation is mediated at least in part by base-base interactions.

The relationship between melting and aggregation in the presence of divalent metal cations has been addressed previously (Knoll et al., 1988; Lin and Chargaff, 1966) and has resulted in two plausible models (Knoll et al., 1988). The first model postulates that aggregation occurs through cross-linking of partially melted duplexes, whereas the second presumes that the duplex remains intact. Our combined results from DSC and Raman spectroscopy suggest that at metal/phosphate ratios of 0.6, the partially melted aggregate

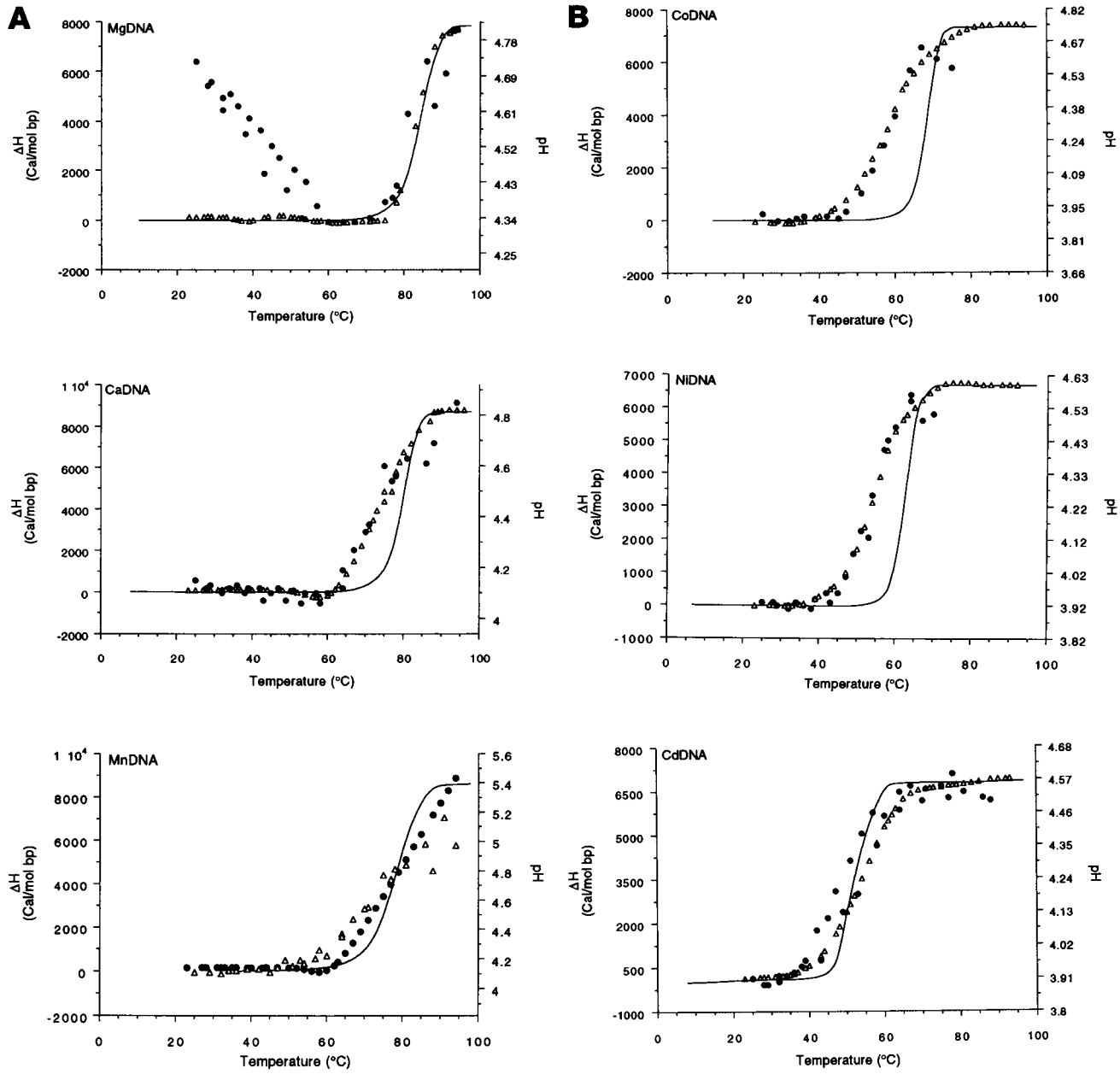

FIGURE 14 Comparative plots of melting (——), aggregation (△), and pH (●) profiles of several DNA-metal complexes: MgDNA, CaDNA, MnDNA, CoDNA, NiDNA, and CdDNA. Solution conditions include 100 mM M^{2+}, 55 mg/ml DNA, and 5 mM sodium cacodylate.

is more likely. Fig. 16 shows a five-step model that explains most of our observations in this study: 1) The divalent cations initially interact with the DNA at phosphate and/or base sites, resulting in proton displacement. 2) A combination of metal-base interactions and heating destabilizes the duplex DNA, causing some of the hydrogen bonds to rupture and base pairs to swing open. This allows divalent metals and protons to bind to additional sites on the DNA bases. 3) Once the DNA bases have swung open, DNA strands that are close to each other can be linked by metal ion bridges, hydrogen bonding, and base stacking. Bases linked by metal ion bridges will probably have sites available for proton binding, provided that the pK_a values of

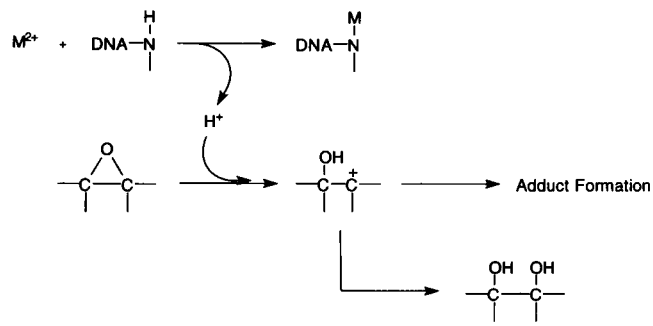

FIGURE 15 Proposed mechanism for metal-induced catalysis of mutagen activation.

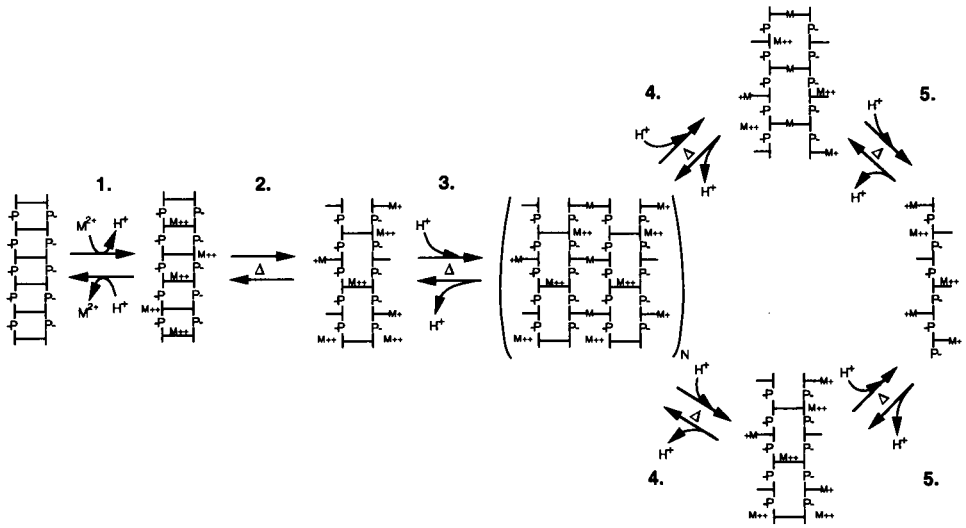

FIGURE 16 Model for DNA aggregation and denaturation in the presence of divalent metal cations. 1, Metal ion binding; 2, base-pair disruption; 3, DNA aggregation; 4, disaggregation; 5, single-strand formation.

these sites are higher than the pH of the solution. This may explain the increase in pH concomitant with aggregate formation. 4) Eventually, near the midpoint of the melting transition, thermal energy breaks up the aggregate. We have no evidence to indicate whether metal ion cross-bridges or direct base-base interactions rupture first. 5) Finally, all cross-links break, resulting in single-stranded DNA complexed with metal ions.

This model seems to explain our experimental observations in a qualitative way. Even better would be a theoretical model to quantify DNA aggregation and denaturation upon heating in the presence of divalent cations. Such a model has been developed (Shibata and Schurr, 1981) for DNA aggregation during thermal denaturation. We have shown (Duguid and Bloomfield, 1995) that this model can be used to explain DNA aggregation and melting in the presence of divalent metal cations. Use of this model enables us to estimate thermodynamic parameters for the elementary steps (ligand binding, disruption of base pairing, and formation of cross-links) in this complex sequence of events.

Because DNA aggregation and melting seem to be related, the same model used to describe ionic strength dependence of thermally induced helix-to-coil transitions (Record et al., 1978) could also be applied to DNA aggregation. It has previously been suggested that the DNA undergoes a B⇆X transition in which the X-form has UV spectral properties similar to those of thermally denatured DNA because of partial base unstacking (Knoll et al., 1988). Calculations using this model showed that the X-form of DNA can become more stable than the B-form under specific conditions of metal ion concentration, linear charge density, and amount of metal bound per phosphate. The experimental observations reported in this paper provide data by which to evaluate ionic concentration and configurational entropy effects on DNA aggregation.

This research was supported by National Institutes of Health grants GM28093 (V.A.B.) and AI18758 (G.J.T.). J.D. was the recipient of a Molecular Biophysics Predoctoral Traineeship from the National Institutes of Health (GM08277) and acknowledges the assistance of R. Becka and K. Reilly (UMKC) and D. Knoll (Kallestad Laboratories, Chaska, MN).

REFERENCES

Anderson, J. A., G. P. P. Kuntz, H. H. Evans, and T. J. Swift. 1971. Preferential interaction of manganous Ions with the guanine moiety in nucleosides, dinucleoside monophosphates, and deoxyribonucleic acid. *Biochemistry.* 10:4368–4374.

Aoki, K. 1976. Crystallographic studies of interactions between nucleotides and metal ions. II. The crystal and molecular structure of the 1:1 complex of cadmium (II) with guanosine 5′-phosphate. *Acta Crystallogr.* B32:1454–1459.

Aubrey, K. L., S. R. Casjens, and G. J. Thomas, Jr. 1992. Secondary structure and interactions of the packaged dsDNA genome of bacteriophage P22 investigated by Raman difference spectroscopy. *Biochemistry.* 31:11835–11842.

Benevides, J. M., P. L. Stow, L. L. Ilag, N. L. Incardona, and G. J. Thomas, Jr. 1991. Differences in secondary structure between packaged and unpackaged single-stranded DNA of bacteriophage ΦX174 determined by Raman spectroscopy: a model for ΦX174 DNA packaging. *Biochemistry.* 30:4855–4863.

Benevides, J. M., A. H.-J. Wang, G. A. van der Marel, J. H. van Boom, and G. J. Thomas, Jr. 1988. Crystal and solution structures of the B-DNA dodecamer d(CGCAAATTTGCGC) probed by Raman spectroscopy: heterogeneity in the crystal structure does not persist in the solution structure. *Biochemistry.* 27:931–938.

Braunlin, W. H., T. Drakenberg, and L. Nordenskiöld. 1987. A ^{43}Ca-NMR study of Ca(II)-DNA interactions. *Biopolymers.* 26:1047–1062.

Braunlin, W. H., L. Nordenskiöld, and T. Drakenberg. 1989. The interaction of calcium(II) with DNA probed by ^{43}Ca-NMR is not influenced by terminal phosphate groups at ends and nicks. *Biopolymers.* 28: 1339–1342.

Breslauer, K. J., R. Frank, H. Blocker, and L. A. Marker. 1986. Predicting DNA duplex stability from the base sequence. *Proc. Natl. Acad. Sci. USA.* 83:3746–3750.

Brown, E. B., and W. L. Peticolas. 1975. Conformational geometry and vibrational frequencies of nucleic acid chains. *Biopolymers.* 14: 1259–1271.

Cantor, C. R., and P. R. Schimmel. 1980. Biophysical Chemistry. Part III. The Behavior of Biological Macromolecules. W. H. Freeman and Co., San Francisco.

Crothers, D. M., N. R. Kallenbach, and B. H. Zimm. 1964. Theory of the melting transition of synthetic polynucleotides: evaluation of the stacking free energy. *J. Mol. Biol.* 9:1–9.

Daune, M. 1974. Interactions of metal ions with nucleic acids. Metal Ions in Biological Systems. 3(High Molecular Weight Complexes). M. Dekker, New York 1–43.

Dix, D. E., and D. B. Straus. 1972. DNA helix stability. 1. Differential stabilization by counter cations. *Arch. Biochem. Biophys.* 152:299–310.

Dove, W. F., and N. Davidson. 1962. Cation effects on the denaturation of DNA. *J. Mol. Biol.* 5:467–478.

Duguid, J., J. M. Benevides, V. A. Bloomfield, and G. J. Thomas, Jr. 1993. Raman spectroscopy of DNA-metal Complexes. I. Interactions and conformational effects of the divalent cations: Mg, Ca, Sr, Ba, Mn, Co, Ni, Cu, Pd, and Cd. *Biophys. J.* 65:1916–1928.

Duguid, J. G., and V. A. Bloomfield. 1995. A model for divalent metal ion mediated crosslinking/aggregation of melted DNA. *Biophys. J.* 69: 2633–2639.

Eichhorn, G. L. 1981. The effect of metal ions on the structure and function of nucleic acids. *In* Metal Ions In Genetic Information Transfer. Elsevier/North Holland, New York.

Eichhorn, G. L., and P. Clark. 1965. Interactions of metal ions with polynucleotides and related compounds. V. The unwinding and rewinding of DNA strands under the influence of copper(II) ions. *Proc. Natl. Acad. Sci. USA.* 53:586–593.

Eichhorn, G. L., and Y. A. Shin. 1968. Interaction of metal ions with polynucleotides and related compounds. XII. The relative effect of various metal ions on DNA helicity. *J. Am. Chem. Soc.* 90:7323–7328.

Erfurth, S. C., E. J. Kiser, and W. L. Peticolas. 1972. Determination of the backbone structure of nucleic acid oligomers by laser Raman scattering. *Proc. Nat. Acad. Sci. USA.* 69:938–941.

Erfurth, S. C., and W. L. Peticolas. 1975. Melting and premelting phenomenon in DNA by laser Raman scattering. *Biopolymers.* 14:247–264.

Gessner, R. V., G. J. Quigley, A. H.-J. Wang, G. A. van der Marel, J. H. van Boom, and A. Rich. 1985. Structural basis for stabilization of Z-DNA by cobalt hexaammine and magnesium cations. *Biochemistry.* 24:237–240.

Hinz, H.-J. 1986. Thermodynamic parameters for protein-protein and protein-ligand interaction by differential scanning microcalorimetry. *Methods Enzymol.* 59–79.

Kasprzak, K. S., and M. P. Waalkes. 1986. The role of calcium, magnesium, and zinc in carcinogenesis. *Adv. Exp. Med. Biol.* 206:497–515.

Keller, P. B., D. M. Loprete, and K. A. Hartman. 1988. Structural forms and transitions of poly(dG-dC) with Cd(II), Ag(I) and $NaN0_3$. *J. Biomol. Struct. Dyn.* 5:1221–1229.

Knoll, D. A., M. G. Fried, and V. A. Bloomfield. 1988. Heat-induced DNA aggregation in the presence of divalent metal salts. *In* Structure and Expression: DNA and Its Drug Complexes. Adenine Press, Albany.

Lafleur, L., J. Rice, and G. J. Thomas, Jr. 1972. Raman studies of nucleic acids. VII. Poly A·poly U and poly G·poly C. *Biopolymers.* 11: 2423–2437.

Lamm, G., and G. R. Pack. 1990. Acidic domains around nucleic acids. *Proc. Natl. Acad. Sci. USA.* 87:9033–9036.

Langlais, M., H. A. Tajmir-Riahi, and R. Savoie. 1990. Raman spectroscopic study of the effects of Ca^{2+}, Mg^{2+}, Zn^{2+}, and Cd^{2+} ions on calf thymus DNA: binding sites and conformational changes. *Biopolymers.* 30:743–752.

Lin, H. J., and E. Chargaff. 1966. On the denaturation of deoxyribonucleic acid. *Biochim. Biophys. Acta.* 123:66–75.

Lord, R. C., and G. C. Thomas, Jr. 1967. Raman studies of nucleic acids. II. Aqueous purine and pryimidine mixtures. *Biochim. Biophys. Acta.* 142:1–11.

Lord, R. C., and G. J. Thomas, Jr. 1968. Spectroscopic studies of molecular interaction in DNA constituents. *Dev. Appl. Spectrosc.* 6:179–199.

Luck, G., and C. Zimmer. 1972. Conformational aspects and reactivity of DNA: effects of manganese and magnesium ions on interaction with DNA. *Eur. J. Biochem.* 29:528–536.

Makrigiannis, G., P. Papagiannakopoulos, and T. Theophanides. 1980. Raman study of metal-guanosine-5′-monophosphate aqueous solutions. *Inorg. Chim. Acta.* 46:263–269.

Mansy, S., G. Y. H. Chu, R. E. Duncan, and R. S. Tobias. 1978. Heavy metal nucleotide interactions. 12. Competitive reactions in systems of four nucleotides with *cis*- or *trans*-diamineplatinum (II). Raman difference spectrophotometric determination of the relative nucleophilicity of guanosine, cytidine, adenosine, and uridine monophosphates as well as the analogous bases in DNA. *J. Am. Chem. Soc.* 100:607–616.

Mansy, S., and R. S. Tobias. 1974. Heavy-metal nucleotide interactions. II. Binding methylmercury(II) to purine nucelosides and nucleotides studied by Raman difference spectroscopy. *J. Am. Chem. Soc.* 96: 6874–6885.

Manzini, G., L. E. Xodo, F. Fogolari, and F. Quadrifoglio. 1990. Secondary structure effects on the interaction of different polynucleotides with Ca^{2+}. *Biopolymers.* 30:325–333.

Marky, L. A., and K. J. Breslauer. 1987. Calculating thermodynamic data for transitions of any molecularity from equilibrium melting curves. *Biopolymers.* 26:1601–1620.

Moller, M. R., M. A. Bruck, T. O'Connor, F. J. Armatis Jr., E. A. Knolinski, N. Kottmair, and R. S. Tobias. 1980. Heavy metal-nucleotide interactions. 14. Raman difference spectrophotometric studies of competitive reactions in mixtures of four nucleotides with the electrophiles methylmercury(II) perchlorate, cis-dimethylgold(III) perchlorate, dichloroethylene-diamine-palladium(II), trans-dichlorodiaminepalladium(II), and aquopentaaminecobalt(III) perchlorate. Factors governing selectivity in the binding reactions. *J. Am. Chem. Soc.* 102:4589–4598.

O'Connor, T., M. Bina, D. R. McMillin, M. R. Moller Haley, and R. S. Tobias. 1982. Heavy metal-nucleotide interactions. 15. Reactions of calf thymus DNA with the electrophiles methylmercury(II) nitrate, *cis*-dichlorodiammineplatinum(II), and *trans*-dichlorodiammineplatinum(II) studied using Raman difference spectroscopy evidence for the formation of C-DNA upon metalation. *Biophys. Chem.* 15:223–234.

Ott, G. S. 1975. The DNA melting transition in aqueous magnesium salt solutions. Ph.D. thesis. University of Colorado, Boulder.

Ott, G. S., D. Bastia, and W. Bauer. 1978. A spectroscopic and electron microscopic examination of the highly condensed DNA structures formed by denaturation in $Mg(ClO_4)_2$. *Biochim. Biophys. Acta.* 518: 216–232.

Prescott, B., W. Steinmetz, and G. J. Thomas, Jr. 1984. Characterization of DNA structures by laser Raman spectroscopy. *Biopolymers.* 23: 235–256.

Privalov, P. L., and S. A. Potakhin. 1986. Scanning microcalorimetry in studying temperature-induced changes in proteins. *Methods Enzymol.* 131:4–51.

Record, T. M. 1975. Effects of Na^+ and Mg^{++} ions on the helix-coil transition of DNA. *Biopolymers.* 14:2137–2158.

Record, M. T., Jr., C. F. Anderson, and T. M. Lohman. 1978. Thermodynamic analysis of ion effects on the binding and conformational equilibria of proteins and nucleic acids: the roles of ion association or release, screening, and ion effects on water activity. *Q. Rev. Biophys.* 11:103–178.

Rimai, L., V. M. Maher, D. Gill, I. Salmeen, and J. J. McCormick. 1974. The temperature dependence of Raman intensities of DNA. Evidence for premelting changes and correlations with ultraviolet spectra. *Biochim. Biophys. Acta.* 361:155–165.

Shibata, J. H., and J. M. Schurr. 1981. A theory of aggregation in the thermal denaturation region of multistrand biopolymers. *Biopolymers.* 20:525–549.

Shimanouchi, T., M. Tsuboi, and Y. Kyogoku. 1964. The structure and properties of biomolecules and biological systems. *In* Advances in Chemical Physics: The Structure and Properties of Biomolecules and Biological Systems. Wiley-Interscience, New York.

Shin, Y. A., and G. L. Eichhorn. 1968. Interactions of metal ions with polynucleotides and related compounds. XI. The reversible unwinding and rewinding of deoxyribonucleic acid by zinc(II) ions through temperature manipulation. *Biochemistry.* 7:1026–1032.

Small, E. W., and W. L. Peticolas. 1971. Conformational dependence of the Raman scattering intensities from polynucleotides. III. Order-disorder changes in helical structures. *Biopolymers.* 10:1377–1416.

Stangret, J., and R. Savoie. 1992. Vibrational spectroscopic study of the interaction of metal ions with diethyl phosphate, a model for biological systems. *Can. J. Chem.* 70:2875–2883.

Strzelecka, T. E., and R. L. Rill. 1987. Solid-state ^{31}P NMR studies of DNA liquid crystalline phases. Isotropic to cholesteric transition. *J. Am. Chem. Soc.* 109:4513–4518.

Sturtevant, J. M. 1987. Biochemical applications of differential scanning calorimetry. *Annu. Rev. Phys. Chem.* 38:463–488.

Tajmir-Riahi, H.-A. 1991. Interaction of guanylic acid with the Mg(II), Ca(II), Sr(II), and Ba(II) ions in the crystalline solid and aqueous solution: evidence for the ribose C2′-endo/anti and C3′-endo/anti conformational changes. *Biopolymers.* 31:101–108.

Tajmir-Riahi, H. A., M. Langlais, and R. Savoie. 1988. A laser Raman spectroscopic study of the interaction of calf-thymus DNA with Cu(II) and Pb(II) ions: metal ion binding and DNA conformational changes. *Nucleic Acids Res.* 16:751–762.

Thomas, G. J., Jr., and J. M. Benevides. 1985. An A-helix structure for poly(dA-dT)·poly(dA-dT). *Biopolymers.* 24:1101–1105.

Thomas, G. J., Jr., and A. H.-J. Wang. 1988. Laser Raman spectroscopy of nucleic acids. *In* Nucleic Acids and Molecular Biology. Springer-Verlag, Berlin.

Van Steenwinkel, R., F. Campagnari, and M. Merlini. 1981. Interaction of Mn^{2+} with DNA as studied by proton-relaxation enhancement of solvent water. *Biopolymers.* 20:915–923.

Wada, A., S. Yabuki, Y. Husimi, and J. G. Brahms. 1980. Fine structure in the thermal denaturation of DNA: high temperature resolution spectrophotometric studies. *CRC Crit. Rev. Biochem.* 9:87–144.

Wang, L., M. Ferrari, and V. A. Bloomfield. 1990. Large-scale preparation of mononucleosomal DNA from calf thymus for biophysical studies. *BioTechniques.* 9:24–27.

Wilcoxon, J., J. M. Schurr, and R. A. J. Warren. 1984. The titratable joint phenomenon in øW-14 DNA. *Biopolymers.* 23:767–774.

Zimmer, C., G. Luck, and H. Triebel. 1974. Conformation and reactivity of DNA. IV. Base binding ability of transition metal ions to native DNA and effect on helix conformation with special reference to DNA-Zn(II) complex. *Biopolymers.* 13:425–453.